Biochemistry

Article

Cite This: *Biochemistry* 2019, 58, 2432−2446

pubs.acs.org/biochemistry

# Hydrogen−Deuterium Exchange Supports Independent Membrane-Interfacial Fusion Peptide and Transmembrane Domains in Subunit 2 of Influenza Virus Hemagglutinin Protein, a Structured and Aqueous-Protected Connection between the Fusion Peptide and Soluble Ectodomain, and the Importance of Membrane Apposition by the Trimer-of-Hairpins Structure

Ahinsa Ranaweera, Punsisi U. Ratnayake, E. A. Prabodha Ekanayaka, Robin Declercq, and David P. Weliky*

Department of Chemistry, Michigan State University, East Lansing, Michigan 48824, United States

Supporting Information

**ABSTRACT:** The influenza virus hemagglutinin (HA) protein has HA1 and HA2 subunits, which form an initial complex. HA1's bind host cell sialic acids, which triggers endocytosis, HA1/HA2 separation, and HA2-mediated fusion between virus and endosome membranes. We report hydrogen−deuterium exchange mass spectrometry (HDX-MS) on the HA2 subunit without HA1. HA2 contains the fusion peptide (FP), soluble ectodomain (SE), transmembrane domain (TM), and endodomain. FP is a monomer by itself, while SE is a trimer of hairpins that includes an interior bundle of residue 38−105 helices, turns, and residue 154−178 strands packed antiparallel to the bundle. FP and TM extend from the same side of the SE hairpin, and fusion models often depict a FP/TM complex with membrane traversal of both domains that is important for membrane pore expansion. The HDX-MS data of this study do not support this complex and instead support independent FP and TM with respective membrane-interfacial and traversal locations. The data also show a low level of aqueous exposure of the 22−38 segment, consistent with retention of the 23−35 antiparallel $\beta$ sheet observed in the initial HA1/HA2 complex. We propose the $\beta$ sheet as a semirigid connector between FP and SE that enables close membrane apposition prior to fusion. The I173E mutant exhibits greater exchange for residues 22−69 and 150−191, consistent with dissociation of SE C-terminal strands from interior N-helices. Similar trends are observed for the G1E mutant as well as less exchange for G1E FP. Fusion is highly impaired with either mutant, which correlates with reduced membrane apposition and, for G1E, FP binding to SE rather than the target membrane.

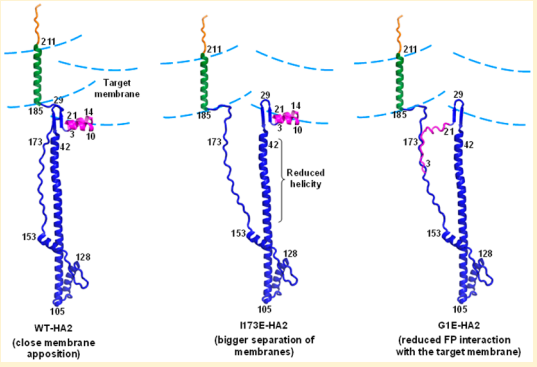




Influenza is an enveloped virus enclosed by a membrane obtained during budding from an infected host cell.[1−3] The viral protein hemagglutinin (HA) is responsible for attachment of the virus to an uninfected host cell and subsequent membrane fusion within the cell. HA is synthesized as a single polypeptide and then proteolytically cleaved into two disulfide-linked subunits, HA1 and HA2, with lengths of ∼330 and ∼220 residues, respectively.[4] HA2 is a single-pass integral membrane protein with an ectodomain (ED) that contains an N-terminal fusion peptide (FP) and soluble ectodomain (SE), a transmembrane domain (TM), and an endodomain (∼25, 160, 25, and 10 residues in length, respectively) (Figure 1A). An initial complex is formed with a HA2 trimeric ED bundle and three HA1's bound to the outside of this bundle.[5,6] The HA1's bind to sialic acids on the host cell surface, which triggers endocytosis. The early endosome with virus cargo migrates to the host cell nucleus and matures with a decrease in its pH to <6, which induces HA1/HA2 separation and HA2 SE rearrangement into a final trimer-of-hairpins structure (Figure 1B).[7,8] A decreased pH also triggers HA-mediated membrane fusion with the following stages: (1) hemifusion in which there is a single bilayer diaphragm that separates the two bodies, (2) pore formation that allows passage of <1 kDa species, and (3) pore expansion that allows deposition of the virus capsid in the cytoplasm.[3,9] Many functional data have been published for pH-triggered fusion between HA-expressing cells (HA-cells) and red blood cells (RBC's).[10,11]

There are high-resolution structures for the initial complex of the proteolytically cleaved HA ED, which includes the HA2 ED

**Received:** December 12, 2018
**Revised:** April 19, 2019
**Published:** April 22, 2019




DOI: 10.1021/acs.biochem.8b01272
*Biochemistry* 2019, 58, 2432−2446

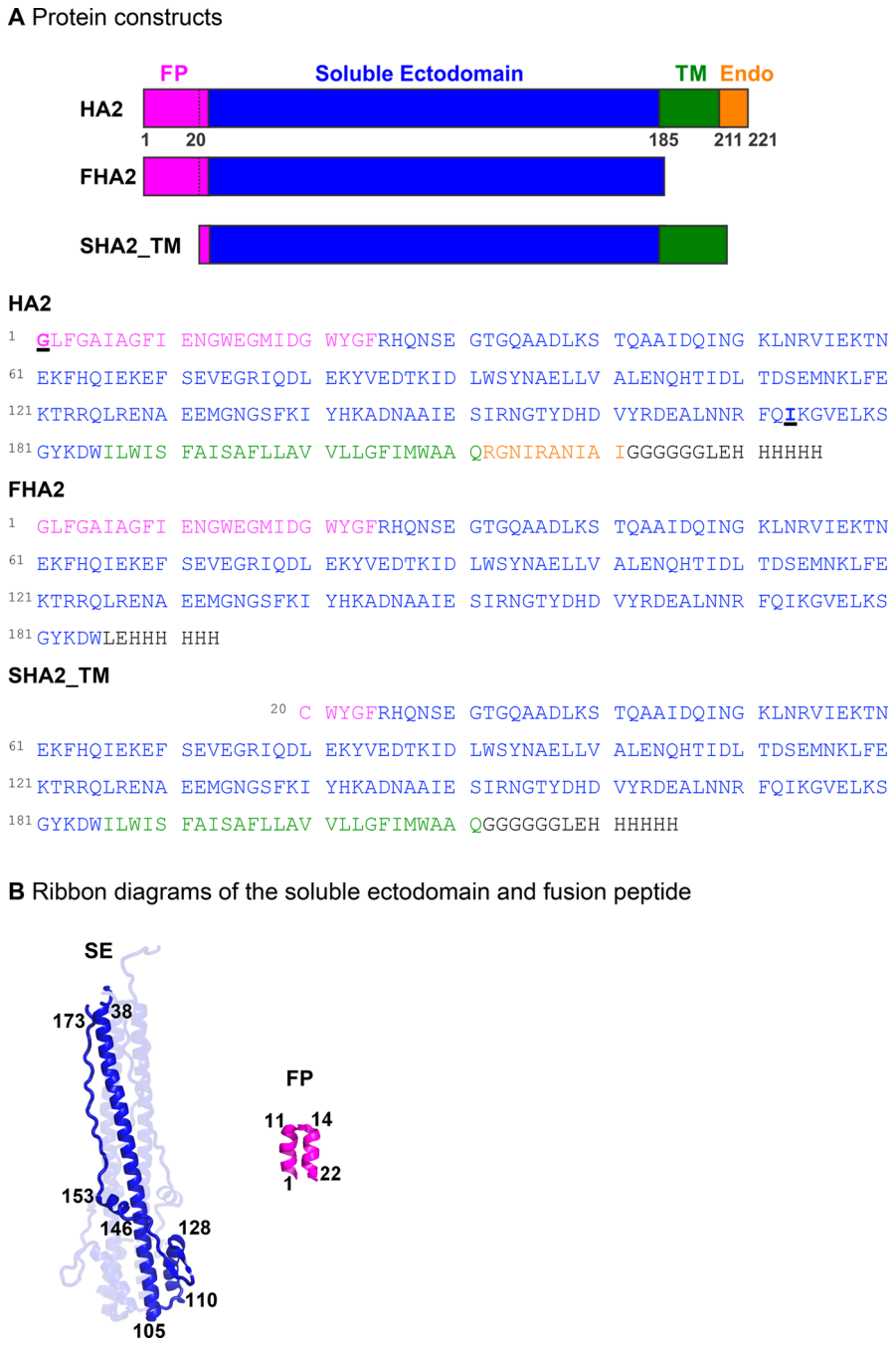


**Figure 1.** (A) Schematic diagrams and sequences of full-length HA2 and truncated constructs with colored domains: pink for the fusion peptide (FP), blue for the soluble ectodomain (SE), green for the transmembrane domain (TM), and orange for the endodomain (Endo). This color coding is also used in Figures 2 and 8. Amino acid sequences are from the X31 strain, which is a H3 subtype. The C-terminal regions (black) include a non-native $H_6$ tag for affinity chromatography. The G1E and I173E mutation sites are underlined in the HA2 sequence. (B) Ribbon diagrams of the SE in the final trimer-of-hairpins structure (PDB entry 1QU1) and the FP with a closed helical hairpin structure (PDB entry 2KXA). A monomer subunit is highlighted for the SE, as well as the terminal residues of regular secondary structure elements, and residue 173.

and HA1. These structures typically show an organization of HA2 ED trimers with three bound HA1's but sometimes show a different organization of individual HA2/HA1 heterodimers.[5,6,12,13] The geometries of the HA2 ED/HA1 units are very similar in either oligomeric organization, which supports the HA2 ED/HA1 heterodimer being a fundamental folding unit. The trimer has a mushroom shape with a stem region containing mostly HA2 and a globular head region containing mostly HA1. The stem includes three $HA2_{76-125}$ helices that form an internal parallel coiled coil pointing away from the head and three $HA2_{38-55}$ helices that are antiparallel to the middle of the coiled coil. The $HA2_{1-20}$ FP's have extended structure buried in the stem and connected to the stem by the $HA2_{23-35}$ $\beta$ sheet hairpins. The $HA2_{130-141}$ segments are also $\beta$ sheet hairpins and connect the stem to the $HA2_{146-153}$ and $HA2_{159-170}$ helices.

There is a topologically distinct structure of the $HA2_{33-178}$ SE without HA1 (Figure 1B). This HA2 structure is hyperthermostable and likely part of the final HA2 fusion state.[14,15] The structure is a trimer of hairpins that includes $HA2_{38-105}$



DOI: 10.1021/acs.biochem.8b01272
*Biochemistry* 2019, 58, 2432−2446

helices in an internal parallel coiled coil, 180° turns, and $HA2_{110-128}$ helices that are antiparallel to and in the grooves of the $HA2_{90-104}$ region of the coiled coil. The $HA2_{130-141}$ $\beta$ sheet hairpins connect to $HA2_{146-153}$ helices that are perpendicular to the internal coiled coil, and the $HA2_{154-178}$ segments have extended structures antiparallel with the $HA2_{38-78}$ segment of the coiled coil. There are limited data about the transformation between the initial and final SE structures, but some data support a functional role for the final trimer-of-hairpins state.[3,16−19] For example, exogenously added HA2 FP+SE constructs induce steps 1 and 2 of "HA0-cell"/RBC fusion, where HA0 is a HA variant that binds to RBC's but does not induce fusion.[20,21] There are striking similarities to HA-cell/RBC fusion, including the requirement of a low pH and a greatly reduced level of fusion for the G1E and I173E mutants that are in the HA2 FP's and SE strands, respectively. There are similar trends with pH and mutations for vesicle fusion induced by full-length HA2 in the final hairpin structure.[14,15] These mutants are examined in the study presented here. The aforementioned data support a model in which HA1 dissociation leads to FP insertion in the target membrane, formation of SE hairpin structure with consequent membrane apposition, and then membrane fusion. An alternate common mechanistic model is membrane fusion with HA2 in intermediate structures that are not the trimer of hairpins, with conversion of some of the free energy released during HA2 structural transformations into activation energy of fusion.[1−3,22] For this model, the final trimer-of-hairpins state forms after fusion is completed and is therefore a "postfusion" state.

The FP sequence is highly conserved across viral subtypes, and its importance in fusion is evidenced by it (and the TM) as the only HA segments that are deeply inserted in the membrane after virus/vesicle fusion.[4,23] HA-cell/RBC fusion is also eliminated by the G1E mutation at the N-terminus of the FP.[11] The FP is initially in the HA2 ED/HA1 trimer in the protein interior and has extended structure but adopts very different structures without the rest of HA2 and HA1 and in detergent-rich or lipid bilayer media.[24−27] For example, $HA2_{1-23}$ in detergent is a monomer and adopts a "closed" helical hairpin structure at both low and neutral pH, with 1−12 helix/tight turn/14−22 helix topology and antiparallel tight packing of the two helices (Figure 1B). In the membrane, there is some population of the closed structure as well as a population of a related "semiclosed" (less tightly packed) structure, with a larger semiclosed:closed population ratio at pH 5 than at pH 7, with a higher level of fusion at the lower pH. The EPR line widths of the spin-labeled FP segment of the trimeric $HA2_{1-127}$ construct bound to the membrane are also consistent with non-interacting monomer FP's. EPR relaxation data correlate with tilted insertion of the FP helices in a single leaflet, with L2 and F3 being ∼12 Å from the membrane phosphorus plane.[28]

This study focuses on hydrogen−deuterium exchange coupled to mass spectrometry (HDX-MS), which is an approach for probing the segmental structure and motion of proteins.[29−32] Incubation of the whole protein in $D_2O$ leads to exchange of backbone N−H for N−D and is followed by pepsin digestion and then MS determination of the percent HDX ($D_{\%}$) of the resultant peptides.[33] The $D_{\%}$ of a peptide is positively correlated with the aqueous exposure, structural disorder, and motion of the corresponding segment of the intact protein. HDX-MS has previously been applied to the HA2 ED (without the TM or the endodomain) in a complex with HA1.[34] Incubation of the complex for 3 h at pH 4.9 followed by HDX/MS at pH 7.4 gave $D_{\%}$ values that were generally consistent with the trimer-of-hairpins structure for the HA2 SE (Figure 1B). For example, the expected protection of the $HA2_{38-105}$ internal helices in this structure correlates with a $D_{\%}$ of <2% for the HA2 53−69 and 70−87 peptides for a 30 min exchange time, and exposure of $HA2_{106-175}$ loops, helices, and strands correlates with a larger $D_{\%}$ of >70% for the HA2 102−109, 100−115, 139−148, 149−167, and 168−175 peptides. Peptides corresponding to the FP segment were not analyzed.

This study describes HDX-MS of HA2 constructs in the absence of HA1, including $HA2_{1-221}$, $HA2_{1-185}$ ≡ FP + SE ≡ "FHA2", and $HA2_{20-211}$ ≡ SE + TM ≡ "SHA2_TM" (Figure 1A).[14,15] Studies of HA2 by itself are relevant because HA2 catalyzes fusion after separation of HA1, and as noted earlier, FHA2 and HA2 (without HA1) induce cell/cell and vesicle fusion. Other new features of this study are inclusion of the TM and endodomain, analysis of FP peptides, and comparison between functional WT and fusion-impaired G1E and I173E mutants. Our study addresses the long-standing hypothesis of a thermostable bundle containing one or more TM helices and the FP helix/helices, with all helices traversing the membrane (Figure 2). This bundle is hypothesized after HA1 dissociation and for late stages of fusion with a role in the final pore expansion step.[1,35−37] The bundle is potentially supported by inhibition of this final but not earlier steps of HA-cell/RBC fusion by truncation of the TM domain.[38] Another potentially supporting observation is full HA-cell/RBC fusion when the HA2 TM and endodomain are replaced by the TM and endodomain of a nonhomologous protein.[39]

Our study also examines the hypothesis that highly impaired fusion for the I173E and G1E mutants is due to dissociation of C-terminal strands of the SE, with consequent destabilization of the N-terminal bundle of the SE (Figure 2). This hypothesis is based on (1) the moderately reduced helicity of I173E versus that of WT or G1E and (2) large and comparable decreases in $T_m$ (≤40 °C) for I173E and G1E versus that of WT, where $T_m$(WT) ≈ 90 °C.[15] Correlation of the stability of the SE trimer of hairpins with fusion supports the importance of membrane apposition by the hairpin prior to fusion. The destabilizing effect of the I173E mutation may be related to the loss of I173 side chain contacts with the N-terminal bundle. G1E destabilization of the SE is surprising because the mutation site is >35 residues from the SE. We hypothesize that G1E destabilizes the FP structure and that destabilized FP's compete with the N-helix bundle of the SE for binding with the C-terminal strands (Figure 2). This is just a hypothesis as there are not yet structural data for G1E.

## MATERIALS AND METHODS

The following reagents and columns were used: *n*-decyl $\beta$-D-maltopyranoside (DM) (Anatrace, Maumee, OH), $D_2O$ (99.9 atom % D) (Cambridge Isotope Laboratories, Andover, MA), and Enzymate BEH pepsin column (2.1 mm × 30 mm), XBridge BEH Vanguard precolumn/trap column (2.1 mm × 5 mm, 2.5 $\mu$m particle size), and C18 column (2.1 mm × 50 mm) (Waters, Milford, MA). Most other reagents were purchased from Sigma-Aldrich (St. Louis, MO). Solvents were high-performance liquid chromatography grade.

Figure 1A displays color-coded domain schematics and amino acid sequences of constructs HA2, FHA2 ≡ $HA2_{1-185}$, and SHA2_TM ≡ $HA2_{20-211}$ (UniProtKB entry P03437). The sequences are from the X31 strain of influenza virus with mutation of all native Cys residues, specifically C137S, C144A, C148A, C195A, C199A, C210A, and C220A. SHA2_TM



DOI: 10.1021/acs.biochem.8b01272
*Biochemistry* 2019, 58, 2432−2446

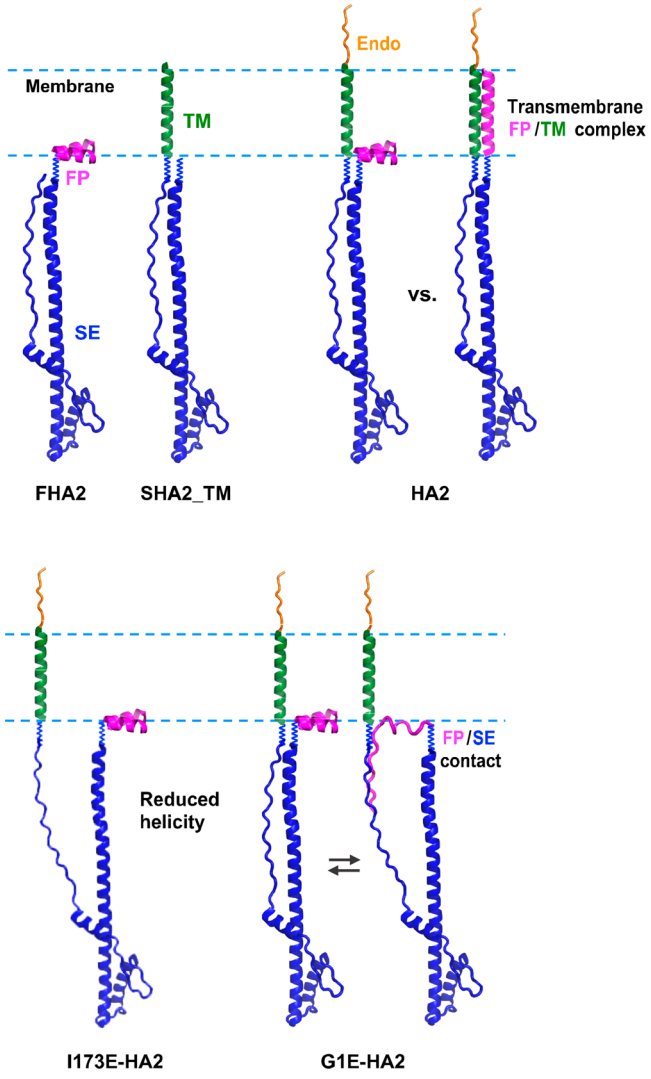


**Figure 2.** Structural models for WT and mutant HA2 constructs that are based on the residue 1−22 FP closed helical hairpin (PDB entry 2KXA), the 36−175 SE hairpin (PDB entry 1QU1), the 186−211 TM continuous $\alpha$ helix that traverses the membrane, and the 212−221 endodomain that is disordered. Residues 23−35 and 176−185 are represented as squiggly lines, because there is not electron density for these residues in PDB entry 1QU1 for all or some of the monomers of the $HA2_{23-185}$ construct. The WT SE is the trimer of hairpins like in Figure 1B, but a single monomer SE is displayed for the sake of clarity. Two WT-HA2 models are shown that have either a FP with a helical hairpin structure at the membrane interface or a FP with continuous $\alpha$ helical structure in complex with a TM and with membrane traversal. I173E-HA2 is shown with dissociated C-terminal SE strands and reduced helicity in the N-terminal SE. This model is consistent with a reduced overall helicity at ambient temperature and a reduced $T_m$ for I173E vs that of WT. G1E-HA2 is shown as an equilibrium between the WT structure and the I173E structure with unfolded FP's that bind the C-terminal SE strands. This model is based on a similar helicity at ambient temperature and a reduced $T_m$ for G1E vs that of WT.

includes an N-terminal G20C mutation introduced for future native chemical ligation (not part of this study). Intertrimer Cys cross-linking is unlikely, based on the absence of such cross-linking in a similar construct of the nonhomologous HIV gp41 protein that also adopts a trimer-of-hairpins structure.[40] There are non-native C-terminal regions $LEG_6H_6$ (HA2 and SHA2_TM) or $LEH_6$ (FHA2) for affinity chromatography. The G1E- and I173E-HA2 constructs were also studied. Preparation of the constructs and expression, purification, and refolding protocols have been previously reported.[15] Protein stocks contained 40 $\mu$M protein in 10 mM Tris-HCl buffer at pH 7.4 with 0.17% DM.

The HDX-MS apparatus included an incubated autosampler (Waters 2777), an external pump (Shimadzu LC-20AD), a UPLC pump system (Waters Acquity Binary Solvent Manager), and a mass spectrometer (Waters Xevo G2S QTof) operating with electrospray ionization in positive ion mode, and continuum mode at $m/z$ 50−2000.[33] HDX was carried out in 1.6 mL capped tubes at 25 °C. The protein stock (6 $\mu$L) was mixed with $D_2O$ buffer (114 $\mu$L), where the latter contained 5 mM HEPES/10 mM MES at pD 7.4 with 0.17% DM. After initial manual mixing, individual tubes were kept without being stirred in the autosampler for either 1, 5, 30, 60, or 120 min. A "0 min" sample was made by mixing with $H_2O$ buffer. After the HDX time, the tube was removed from the autosampler and 120 $\mu$L of ice-cold formic acid (FA) was added, so that pH was decreased to <3, which inhibited additional HDX. Back "DHX" exchange was minimized by the surrounding ice around the tube and around other solutions, injection ports, valves, and columns.

The next set of liquid transfers was performed with the external pump. Protein digestion was performed in a pepsin column that had been equilibrated with a flow of water with 0.1% FA ($H_2O_{FA}$). The protein solution (100 $\mu$L) was transferred to the column using a 0.1 mL/min flow, followed by digestion in the column for 1 min. The solution was then transferred to the trap column using a 0.5 mL/min flow, followed by desalting with a 1 min flow of $H_2O_{FA}$. Flow control was transferred to the UPLC system, and the flow rate set to 0.3 mL/min. The flow then went from the trap column to the C18 column, and the peptides were separated using mixtures of $H_2O_{FA}$ and acetonitrile with 0.1% FA ($ACN_{FA}$). The following separation program was used: 1% $ACN_{FA}$ (1 min), a gradient to 30% $ACN_{FA}$ (3 min), a second gradient to 99% $ACN_{FA}$ (3 min), and 99% $ACN_{FA}$ (1 min). The flow from the column went to the mass spectrometer for analysis.

The protocol described above was first applied to the "0 min" sample prepared by mixing with $H_2O$ buffer. Individual $m/z$ peak distributions in the mass spectrum were assigned to specific peptide sequences by manual comparison of the average natural-abundance mass ($M_H$) of the distribution with theoretical $M_H$'s. Assignments were confirmed by MS/MS analysis. The mass spectra of HDX samples were assigned by the same procedure. Peaks assigned to a single peptide within a user-selected $m/z$ window were inputs for the HX-Express software, which then calculated the peak area weighted-average $m/z$ for each $t_{HDX}$.[41] The outputs were the average $M_H$ ($t_{HDX} = 0$) and average $M_D$ at each $t_{HDX}$ that was greater than zero. For a particular peptide, the percent deuterium incorporation $D_{\%}(t) = 100 \times [M_D(t) - M_H]/N$, where $N$ is the number of backbone amide hydrogens in the peptide.

## RESULTS AND DISCUSSION

Figure S1 displays sequence coverages for identified peptides from the different constructs. For all constructs, there is >90% coverage of the HA2 region of the sequence. Figure 3 displays mass spectra versus $t_{HDX}$ for representative peptides of WT-FHA2, SHA2_TM, and HA2, and Figure 4 displays $D_{\%}$ vs $\log_{10}(t_{HDX}/\text{min})$ for all peptides of these constructs. Figures 5 and 6 display similar plots for WT-, G1E-, and I173E-HA2. The HA2 data in Figures 3 and 4 are the same as the WT-HA2 data in


DOI: 10.1021/acs.biochem.8b01272
Biochemistry 2019, 58, 2432−2446

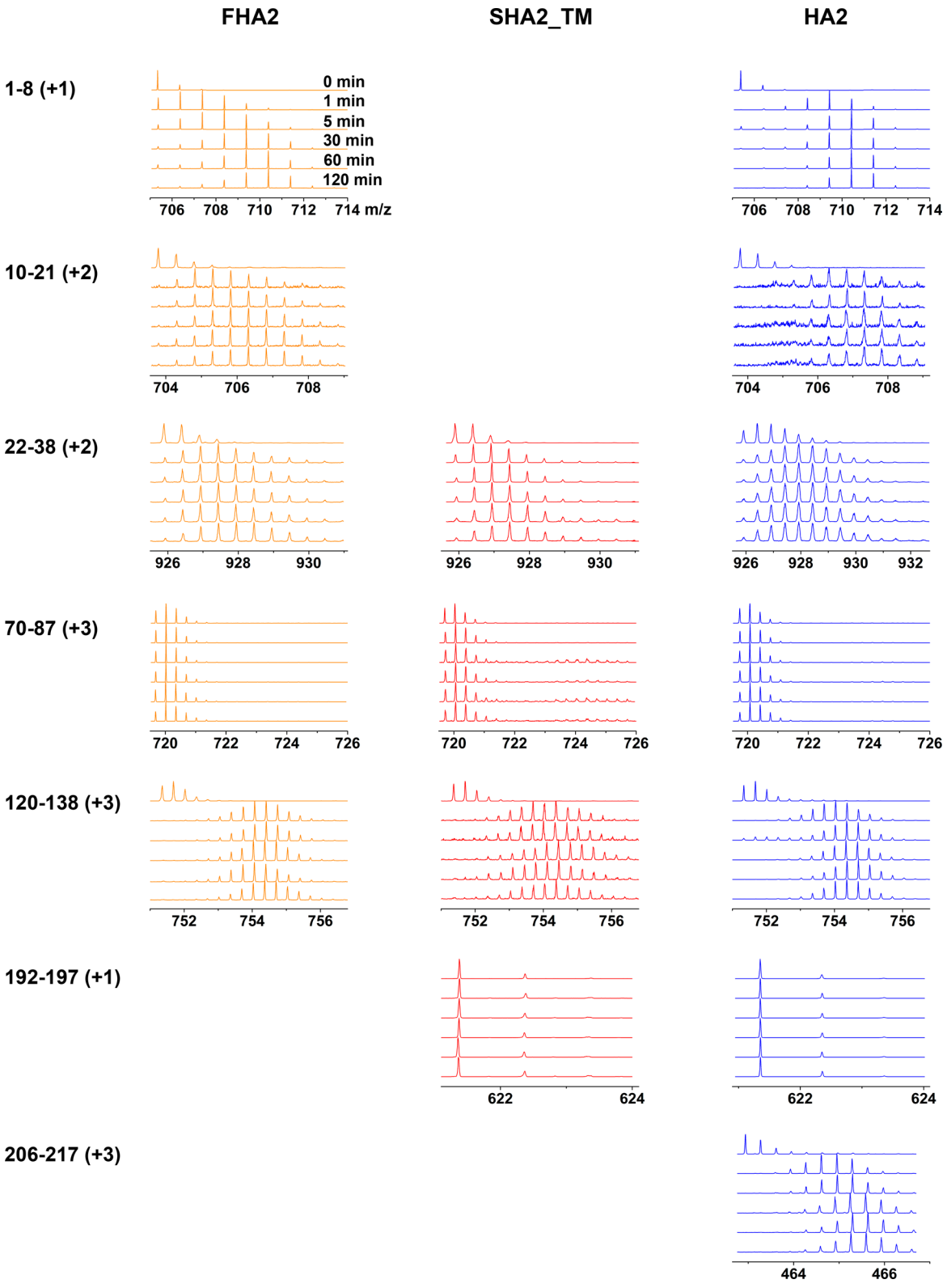


**Figure 3.** HDX-MS data for selected peptides of FHA2, SHA2_TM, and HA2 proteins in DM detergent. Plots of the mass spectral signal intensity vs $m/z$ are displayed for all values of $t_{HDX}$ (the incubation time of the protein in buffer with $D_2O$). The identity and charge of each peptide are given in the left column, with identities confirmed by MS/MS analysis. The shifts of the distributions to larger $m/z$ values with $t_{HDX}$ reflect an increasing level of H → D substitution in the segment of the protein corresponding to the peptide.

Figures 5 and 6. Use of $\log_{10}(t_{HDX})$ for the horizontal axis is for clarity of presentation and is not based on a specific kinetic model of HDX. The maximum $D_{\%}$ values are ~70% rather than 100%, which is consistent with some structure in all regions other than the $HA2_{212–221}$ endodomain and may also reflect some reduction in $D_{\%}$ due to DHX back-exchange during the ~10 min digestion and chromatographic separation steps.[31] Back-exchange is estimated using the 62% experimental



DOI: 10.1021/acs.biochem.8b01272
*Biochemistry* 2019, 58, 2432–2446

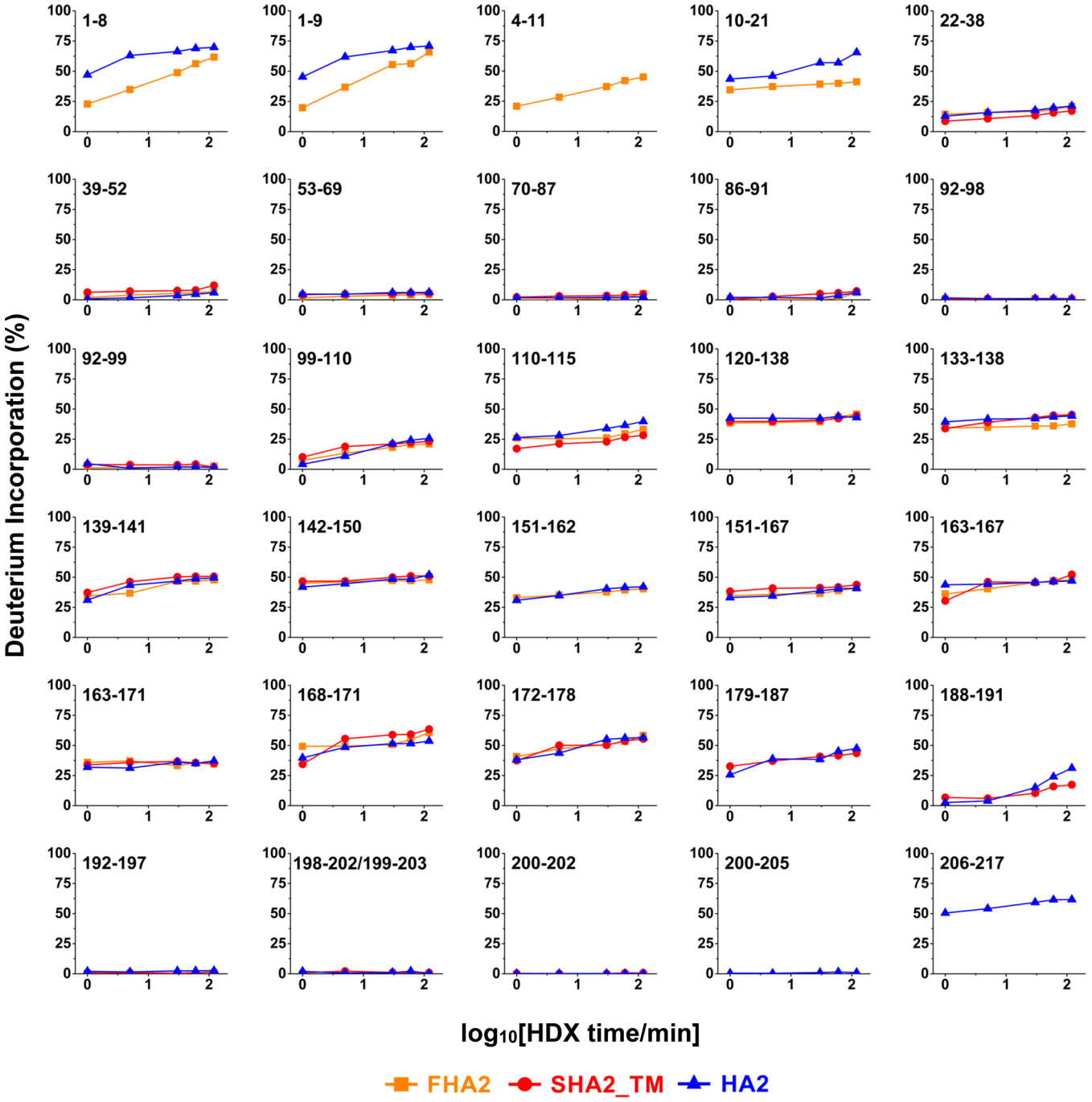


**Figure 4.** Plots of percent deuterium incorporation ($D_{\%}$) vs $\log_{10}(t_{HDX}/\text{min})$ for all analyzed peptides of FHA2, SHA2_TM, and HA2. Peak intensities vs $m/z$ (Figure 3) are inputs for the HX-Express software, which calculates peak area weighted-average $m/z$ values, denoted $M_H$ for dilution into $H_2O$ buffer or $M_D(t)$ for dilution into $D_2O$ buffer for duration $t \equiv t_{HDX}$. $D_{\%}(t) = 100 \times [M_D(t) - M_H]/N$, where $N$ is the number of backbone amide hydrogens in the peptide. Each point in a plot is the average of triplicate measurements, with a typical RMSD of 1%. Table S1 lists all $D_{\%}(t)$ values and associated replicate uncertainties.

exchange at 2 h for $HA2_{206-217}$. The 212−217 fragment in the endodomain likely exhibits full exchange, whereas the 207−211 fragment in the TM is estimated to have 35−40% exchange based on 48% and 31% values for $HA2_{179-187}$ and $HA2_{188-191}$, respectively, that include residues from the other end of the TM. The calculated exchange for the 212−217 fragment is ∼80%, which implies ∼20% back-exchange. Informative conclusions can still be drawn from our data based on significant variations in the $D_{\%}$ values of different peptides of the same construct and variations in the $D_{\%}$ values for the same peptide in different constructs.

Tables 1 and 2 present $\langle D_{\%} \rangle$ for the peptides, where $\langle D_{\%} \rangle$ is the average of all $t_{HDX}$ data, i.e., 1, 5, 30, 60, and 120 min. The uncertainties are in parentheses with typical values of 0.5% that are calculated using the root-mean-square deviations (RMSD's) of the $D_{\%}$ values. Although $\langle D_{\%} \rangle$ does not have a specific physical meaning, $\langle D_{\%} \rangle$ is a convenient single number for describing each peptide. Figure 7 displays the models of Figure 2 with colors based on the $\langle D_{\%} \rangle$ values from Tables 1 and 2.



DOI: 10.1021/acs.biochem.8b01272
*Biochemistry* 2019, 58, 2432−2446

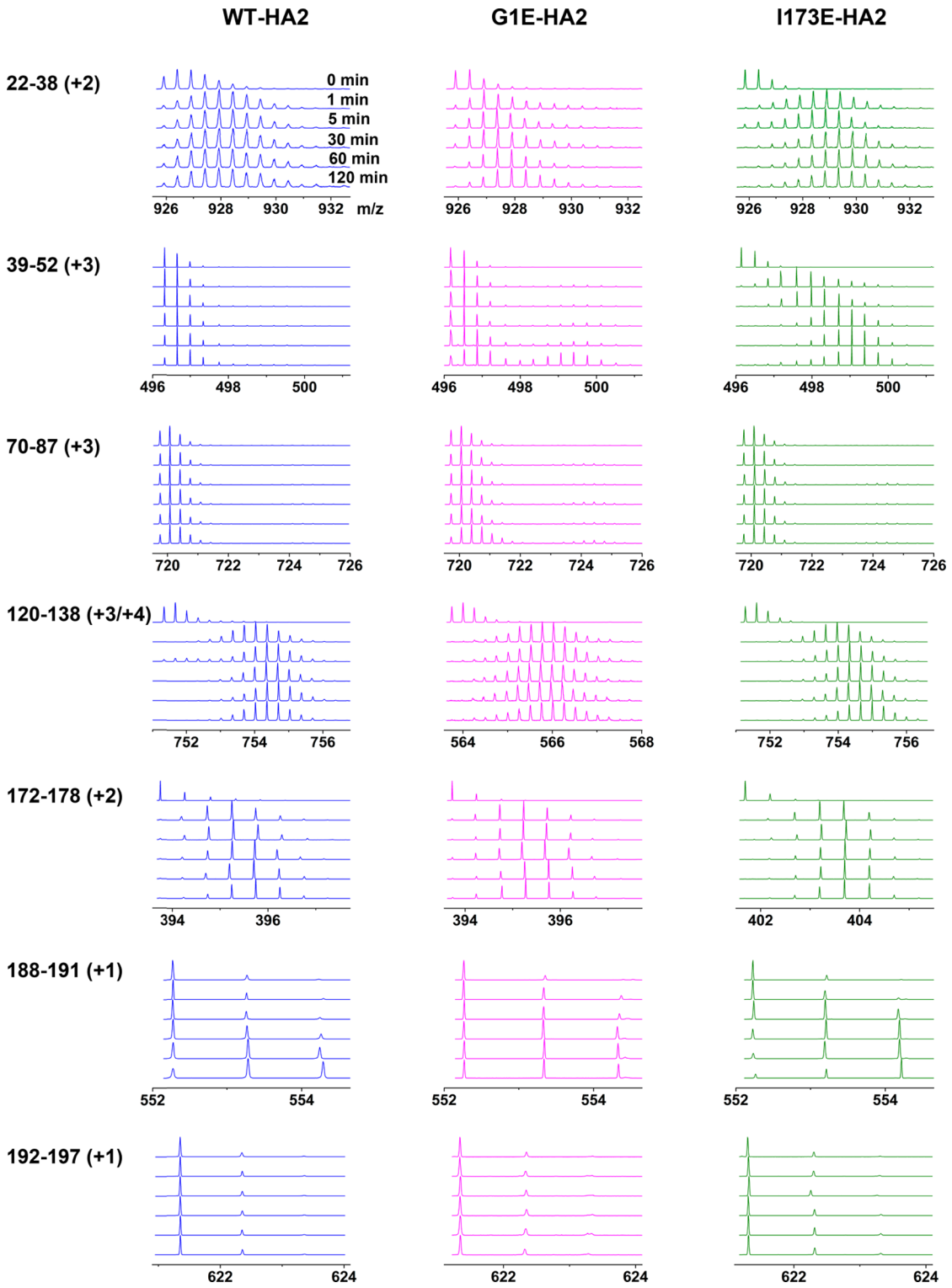


**Figure 5.** HDX-MS data for selected peptides of WT-, G1E-, and I173E-HA2 proteins in DM detergent. Plots of mass spectral signal intensity vs $m/z$ are displayed for all $t_{HDX}$ (the incubation time of the protein in buffer with $D_2O$). The identity and charge of each peptide are given in the left column, with identities confirmed by MS/MS analysis. The shifts of the distributions to larger $m/z$ values with $t_{HDX}$ reflect an increasing level of H → D substitution in the segment of the protein corresponding to the peptide.

**The WT Structural Model Supports the Significance of Membrane Apposition during Fusion.** Figure 8 (left) displays a structural model for WT-HA2 that is based on integration of the HDX-MS data of this study and high-resolution structures of segments of HA2. The FP and TM in Figure 8 are in the different membranes that exist prior to fusion, but no significant changes in protein structure are expected when the FP and TM are in a single membrane after fusion. Figure S2 displays the HA2 structures in a single membrane. One caveat of the membrane interpretation of our HDX-MS data is that our samples are in DM detergent. However, DM is probably a reasonable membrane mimetic, as evidenced by well-



DOI: 10.1021/acs.biochem.8b01272
*Biochemistry* 2019, 58, 2432−2446

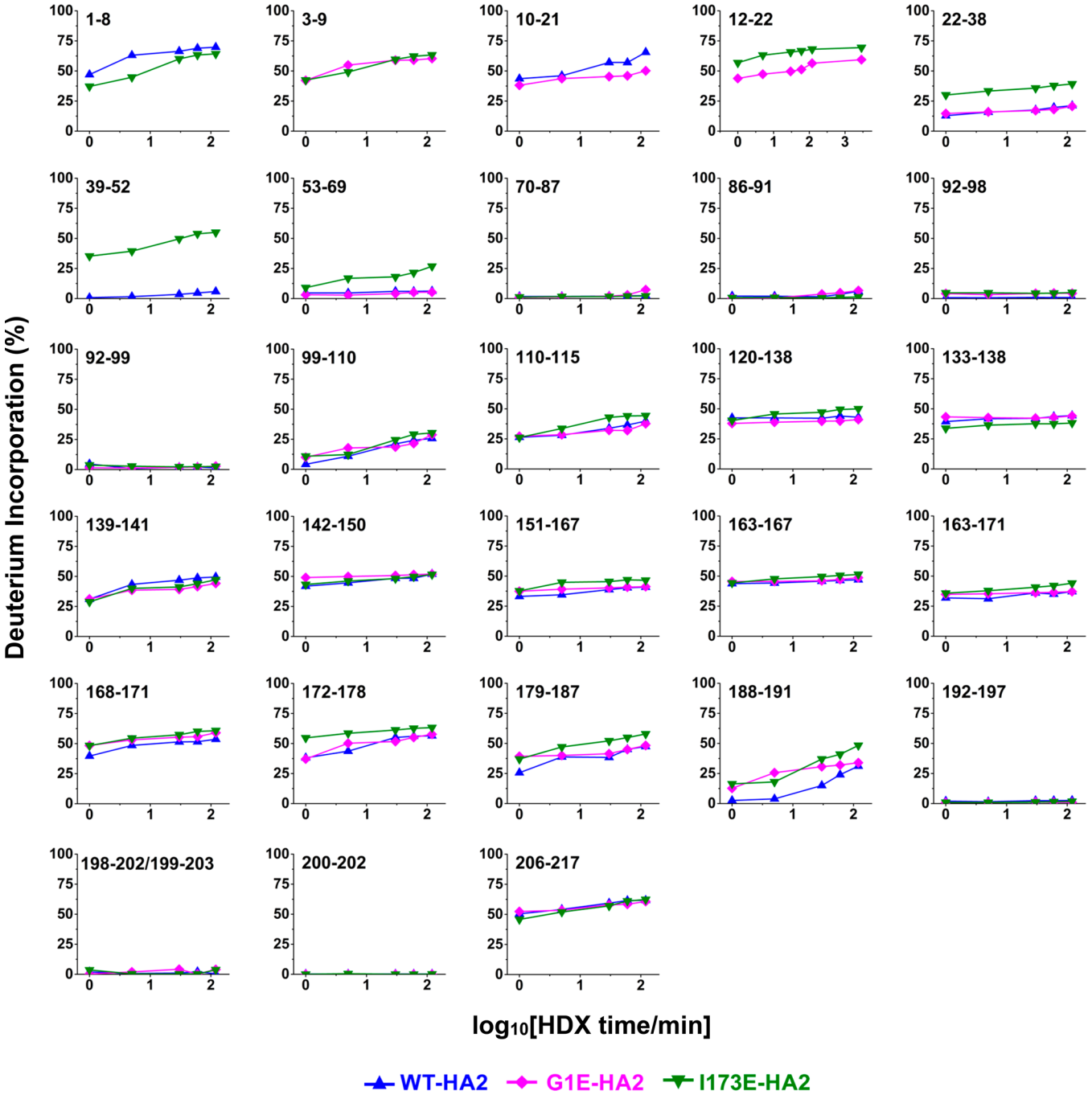


**Figure 6.** Plots of percent deuterium incorporation ($D_{\%}$) vs $\log_{10}(t_{HDX}/\text{min})$ for all analyzed peptides of WT-, G1E-, and I173E-HA2. Peak intensities vs $m/z$ (Figure S) are inputs for the HX-Express software, which calculates peak area weighted-average $m/z$ values, denoted $M_H$ for dilution into $H_2O$ buffer or $M_D(t)$ for dilution into $D_2O$ buffer for duration $t \equiv t_{HDX}$. $D_{\%}(t) = 100 \times [M_D(t) - M_H]/N$, where $N$ is the number of backbone amide hydrogens in the peptide. Each point in a plot is the average of triplicate measurements, with a typical RMSD of 1%. Table S2 lists all $D_{\%}(t)$ values and associated replicate uncertainties.

folded, hyperthermostable, and fusion-active protein in DM.[15] For simplicity of presentation, we subsequently refer to only the membrane. The model in Figure 8 includes the trimer-of-hairpins SE structure shown in Figure 1B and is supported by HDX-MS data for HA2, FHA2, and SHA2_TM (Figures 3, 4, and 7), with typical $\langle D_{\%} \rangle$ of <5% for 39−99 peptides from the trimer interior and 35−50% for 110−178 peptides from the hairpin turns and trimer exterior. For the sake of clarity, Figure 8 shows only one monomer unit of the trimer. The FP and TM in Figure 8 are displayed as independent domains with respective membrane-interfacial and traversal locations. These locations are based on $\langle D_{\%} \rangle$ values of >35% for the 1−21 fragment and <3% for the 192−205 fragment. The data do not support a transmembrane FP/TM complex, for which the $\langle D_{\%} \rangle$ for the FP would be small and comparable with that of the TM (Figure 2). The extensive exchange for the FP is more consistent with monomer than with oligomer FP's, whereas complete protection of the TM is consistent with either monomer or oligomer TM's that traverse the membrane. The $\langle D_{\%} \rangle$ of 57% for the 206−217



DOI: 10.1021/acs.biochem.8b01272
*Biochemistry* 2019, 58, 2432−2446

Table 1. $\langle D_{\%} \rangle$ Values for Peptides from FHA2, SHA2_TM, and HA2[a]

| peptide | FHA2 | SHA2_TM | HA2 |
|---|---|---|---|
| 1−8 | 44.88(0.58) | | 63.02(0.52) |
| 1−9 | 46.82(0.40) | | 63.03(0.94) |
| 10−21 | 38.43(0.68) | | 53.88(0.31) |
| 4−11 | 34.67(0.76) | | |
| 22−38 | 17.19(0.61) | 13.13(0.55) | 17.43(0.66) |
| 39−52 | 4.74(0.35) | 8.12(0.13) | 3.26(0.23) |
| 53−69 | 3.33(0.34) | 5.05(0.29) | 5.50(0.23) |
| 70−87 | 1.66(0.78) | 3.47(0.15) | 2.01(0.06) |
| 86−91 | 1.81(0.42) | 4.16(0.55) | 3.02(0.54) |
| 92−98 | 0.82(0.06) | 0.74(0.12) | 1.09(0.39) |
| 92−99 | 1.73(0.29) | 3.44(0.18) | 2.18(0.25) |
| 99−110 | 16.10(0.35) | 19.05(0.52) | 17.21(0.22) |
| 110−115 | 28.04(0.70) | 23.19(0.65) | 32.87(0.36) |
| 120−138 | 41.29(0.54) | 41.40(0.96) | 42.81(0.87) |
| 133−138 | 35.72(0.54) | 41.17(0.31) | 42.20(0.51) |
| 139−141 | 42.43(0.49) | 47.03(0.55) | 43.88(0.96) |
| 142−150 | 46.68(0.83) | 49.13(0.54) | 47.04(0.04) |
| 151−162 | 37.14(0.65) | | 37.95(0.38) |
| 151−167 | 37.41(0.76) | 41.21(0.66) | 37.50(0.56) |
| 163−167 | 43.33(0.71) | 44.20(0.68) | 45.43(0.34) |
| 163−171 | 35.26(1.07) | 35.38(0.83) | 34.27(0.83) |
| 168−171 | 52.98(0.73) | 54.26(0.55) | 48.97(0.87) |
| 172−178 | 50.03(0.45) | 49.36(0.98) | 49.85(0.67) |
| 179−187 | | 39.10(0.47) | 39.07(0.54) |
| 188−191 | | 11.27(0.54) | 15.31(0.13) |
| 192−197 | | 2.59(0.32) | 2.19(0.17) |
| 198−202/199−203 | | 1.19(0.28) | 1.24(0.42) |
| 200−202 | | 0.40(0.24) | 0.13(0.11) |
| 200−205 | | | 0.89(0.13) |
| 206−217 | | | 57.41(1.04) |

[a] $\langle D_{\%} \rangle$ is the average $D_{\%}$ for $t_{HDX}$ = 1, 5, 30, 60, and 120 min (see Figure 4 and Table S1). The numbers in parentheses are the calculated uncertainties.

Table 2. $\langle D_{\%} \rangle$ Values for Peptides from WT-, G1E-, and I173E-HA2[a]

| peptide | WT-HA2 | G1E-HA2 | I173E-HA2 |
|---|---|---|---|
| 1−8 | 63.02(0.52) | | 53.89(0.74) |
| 3−9 | | 55.09(1.00) | 55.33(1.45) |
| 10−21 | 53.88(0.31) | 44.68(0.70) | |
| 12−22 | | 49.79(1.14) | 63.18(1.19) |
| 22−38 | 17.43(0.66) | 17.29(0.57) | 35.23(0.42) |
| 39−52 | 3.26(0.23) | | 47.00(0.87) |
| 53−69 | 5.50(0.23) | 4.12(0.51) | 18.44(0.41) |
| 70−87 | 2.01(0.06) | 2.93(0.41) | 1.75(0.11) |
| 86−91 | 3.02(0.54) | 3.16(0.54) | 0.90(0.22) |
| 92−98 | 1.09(0.39) | 4.12(0.21) | 4.64(0.12) |
| 92−99 | 2.18(0.25) | 1.92(0.59) | 2.74(0.58) |
| 99−110 | 17.21(0.22) | 19.32(0.53) | 21.40(0.92) |
| 110−115 | 32.87(0.36) | 31.43(0.77) | 38.17(0.98) |
| 120−138 | 42.81(0.87) | 39.47(0.44) | 46.49(0.77) |
| 133−138 | 42.20(0.51) | 43.02(0.39) | 36.69(0.40) |
| 139−141 | 43.88(0.96) | 38.90(0.46) | 40.22(1.05) |
| 142−150 | 47.04(0.04) | 50.58(0.29) | 47.77(0.61) |
| 151−167 | 37.50(0.56) | 39.77(0.16) | 44.26(0.85) |
| 163−167 | 45.43(0.34) | 46.64(0.41) | 48.70(0.71) |
| 163−171 | 34.27(0.83) | 35.99(0.90) | 40.11(0.71) |
| 168−171 | 48.97(0.87) | 54.33(1.51) | 56.21(0.82) |
| 172−178 | 49.85(0.67) | 50.34(0.53) | 60.05(0.81) |
| 179−187 | 39.07(0.54) | 42.79(0.96) | 49.78(0.94) |
| 188−191 | 15.31(0.13) | 27.00(1.10) | 32.11(1.11) |
| 192−197 | 2.19(0.17) | 1.07(0.17) | 1.31(0.10) |
| 198−202/199−203 | 1.24(0.42) | 2.13(1.12) | 1.62(0.85) |
| 200−202 | 0.13(0.11) | 0.00(0.00) | 0.13(0.06) |
| 206−217 | 57.41(1.04) | 56.56(0.45) | 55.63(1.00) |

[a] $\langle D_{\%} \rangle$ is the average $D_{\%}$ for $t_{HDX}$ = 1, 5, 30, 60, and 120 min (see Figure 6 and Table S2). The numbers in parentheses are the calculated uncertainties.

region is consistent with a contribution from an aqueous-exposed and structurally disordered $HA2_{212-221}$ endodomain.

Figure 8 displays the 23−35 region as a 23−27 strand/28−30 turn/31−35 strand antiparallel $\beta$ sheet. The $HA2_{1-175}$/HA1 structure contains this motif; by contrast, the $HA2_{23-185}$ ED structure does not have clear electron density in the 23−33 region, and $HA2_{1-28}$ does not exhibit NMR signals for residues 25−28. The latter observations are reasonably interpreted to support a flexible and disordered 23−35 region of HA2 with a high level of aqueous exposure and an expected $\langle D_{\%} \rangle$ of >50%. It was therefore unexpected that $\langle D_{\%} \rangle_{22-38}$ equaled 17% for HA2 and FHA2 and 13% for SHA2_TM, with 0.6% uncertainties in individual $\langle D_{\%} \rangle_{22-38}$ values. For comparison, $\langle D_{\%} \rangle_{39-52}$ values are ∼4% and 8%, respectively, where the 39−52 fragment is on the interior of the trimer of hairpins. The small $\langle D_{\%} \rangle_{22-38}$ values are consistent with a well-structured and aqueous-protected region and are the basis for the proposed retention of the 23−35 $\beta$ sheet hairpin in the final state of HA2 without HA1. The 23−35 sequence is reasonably conserved across the subtypes of hemagglutinin and likely is not deeply membrane-inserted, on the basis of a few hydrophobic residues.[4] Figure 8 also shows a 179−185 bend region like that in one of the six monomers of the $HA2_{23-185}$ crystal structure; the remaining monomers do not have electron density for most of these residues. The bend in all monomer units is consistent with smaller values of $\langle D_{\%} \rangle$ of 39% for residues 179−187 and 50% for residues 172−178, where the latter is a well-structured segment on the exterior of the SE trimer of hairpins.

Figure 8 provides a mechanistic basis for the observation that HA2 in its final SE hairpin state without HA1 catalyzes cell/cell and vesicle fusion, and we propose that the mechanism is also relevant for virus/endosome fusion. For this mechanism, the entire 23−185 ED provides a semirigid and hyperthermostable connection between the FP and TM that ensures close apposition of the two membranes prior to fusion and compensates for much of the ∼60 kT (computed) activation barrier between the initial two-membrane state and the first "stalk" fusion intermediate.[3] Subsequent hemifusion and pore formation steps have much lower computed activation barriers.

We also use our model in Figure 8 to understand earlier observations that the TM is necessary for the final pore expansion step of HA-cell/RBC fusion and that efficient fusion occurs with replacement of the HA2 TM with a TM sequence of a nonhomologous protein.[39,42] The HDX-MS data do not support a FP/TM complex, so the TM segments on their own might facilitate pore expansion by shielding acyl chains of lipids from water during their transition from the hemifusion diaphragm separating the two bodies to the final continuous bilayer enclosing the fused body. In addition, the membrane location of both the FP and TM with the semirigid HA2 ED structure may lead to positive membrane curvature (see Figure S2 for HA2 with FP and TM in a single membrane). This



DOI: 10.1021/acs.biochem.8b01272
Biochemistry 2019, 58, 2432−2446

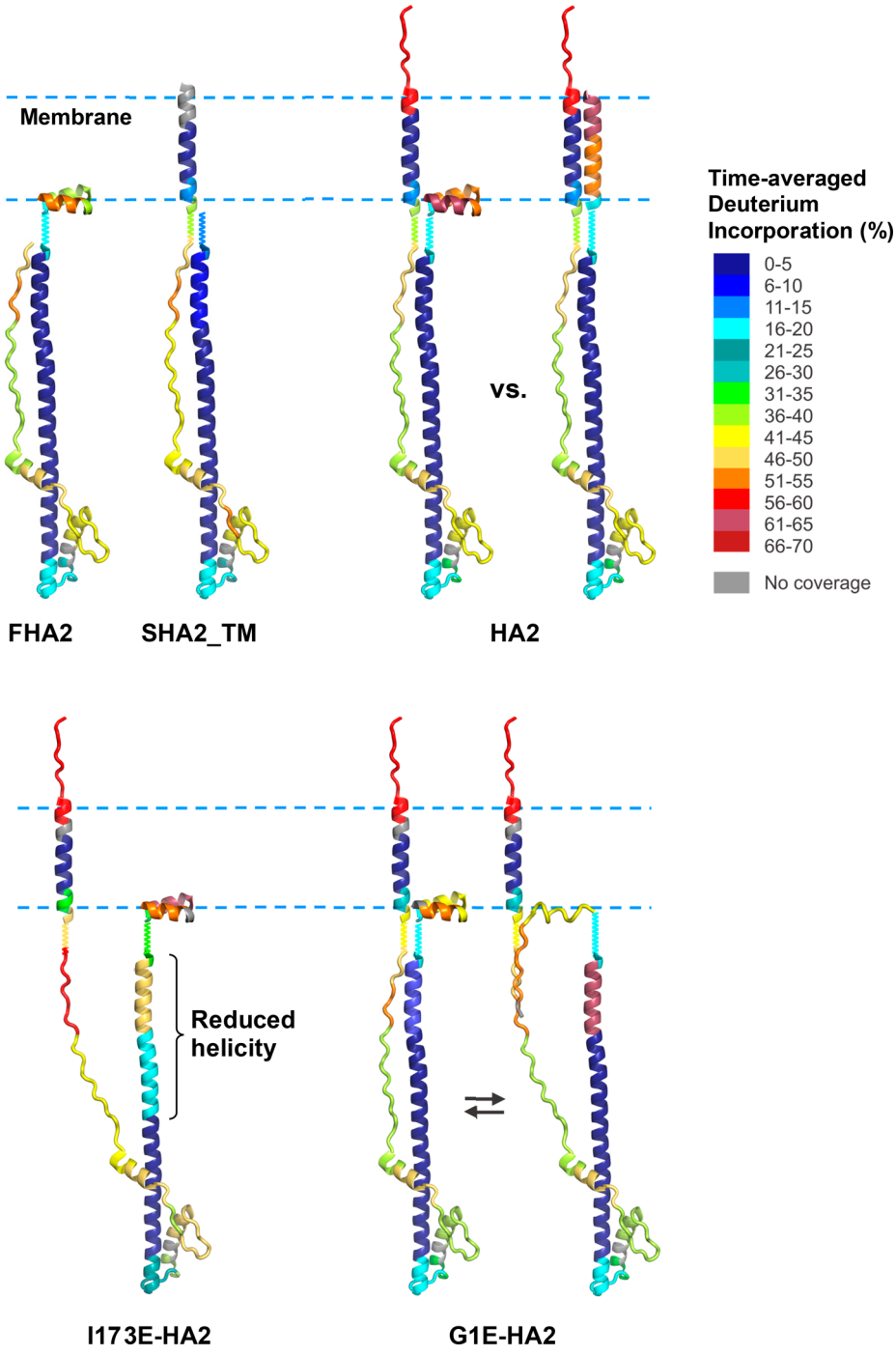


**Figure 7.** Presentation of peptide $\langle D_{\%} \rangle$ from Tables 1 and 2 using color coding and the structural models of Figure 2. The colors for WT-HA2 are based on the $\langle D_{\%} \rangle$ values of peptides 1−9, 10−21, 22−38, 39−52, 53−69, 70−87, 86−91, 92−98, 99−110, 110−115, 120−138, 139−141, 142−150, 151−167, 168−171, 172−178, 179−187, 188−191, 192−197, 198−202, 200−205, and 206−217. The colors for other constructs are based on the $\langle D_{\%} \rangle$ values of subsets of these peptides with a few substitutions that include residues 3−9 for G1E-HA2 and residues 1−8 and 12−22 for I173E-HA2.

curvature may aid pore expansion, which typically has an associated increase in positive curvature. Deletion of TM from HA2 would probably release curvature stress and allow deeper FP membrane insertion. The latter prediction correlates with the smaller $\langle D_{\%} \rangle$ for the FP in FHA2 versus HA2; e.g., $\langle D_{\%} \rangle_{1-8}$ values of 45% versus 63% and $\langle D_{\%} \rangle_{10-21}$ values of 54% versus 38%. Deletion of the FP may also result in deeper insertion of the protein, which correlates with smaller $\langle D_{\%} \rangle_{22-38}$ values and smaller $\langle D_{\%} \rangle_{188-191}$ values for SHA2_TM versus HA2; i.e., 13% versus 17% and 11% versus 15%, with typical uncertainties of ≈0.5%.

**Structural Destabilization of I173E- and G1E-HA2 Underlies Their Fusion Impairment.** Figure 8 (center) displays a structural model for I173E-HA2 that is supported by our HDX-MS data. The I173E structure is the same as that of WT in the FP, 70−150 SE, TM, and endodomain regions, as supported by the similar $\langle D_{\%} \rangle$ values of I173E and WT for the 1−8, 70−99, 120−150, and 192−217 segments. The C-terminal strand of I173E is dissociated from the N-terminal bundle with a



DOI: 10.1021/acs.biochem.8b01272
*Biochemistry* 2019, 58, 2432−2446

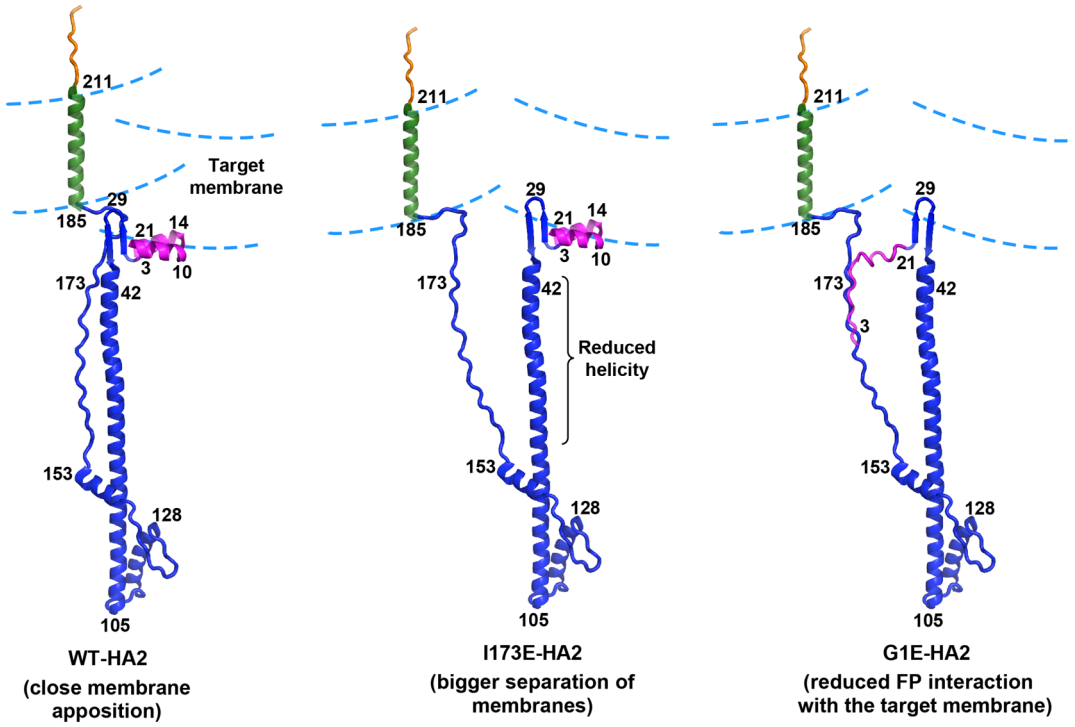


**Figure 8.** Structural models for WT-, I173E-, and G1E-HA2 developed using the HDX-MS data of this study. The proteins are bound to two membranes prior to fusion using color coding of domains like in Figures 1 and 2. WT has a trimer-of-hairpins structure for the SE as in Figure 1B, but only one monomer is shown for the sake of clarity. The approximate positions of specific residues are indicated by the numbers. The WT model combines the residue 1−22 closed FP helical hairpin (PDB entry 2KXA), the 23−35 antiparallel $\beta$ sheet of the $HA2_{1-175}$/HA1 complex (PDB entry 2HMG), the 36−178 hairpin SE structure (PDB entry 1QU1), the 186−211 continuous $\alpha$ helix for TM, and the 212−221 unstructured endodomain. The 179−185 extended structure is found in one monomer in PDB entry 1QU1, but there is not electron density for these residues in the other two monomers. The TM traverses the virus membrane; the FP is interfacially bound to the target membrane, and the membranes are held in close apposition by the fully structured and semirigid 23−185 SE. The close apposition reduces the activation energy for fusion. The HDX-MS data support new features in Figure 8 vs those in Figure 2 that include the 23−35 $\beta$ sheet, 179−185 structure, and respective membrane-interfacial and traversal locations of the FP and TM rather than the FP/TM complex in Figure 2. The structure in Figure 8 is retained in the final fused membrane, which has local positive curvature that accommodates the FP and TM locations (see Figure S2) and may be important for fusion pore expansion. The I173E model shows dissociation of the C-terminal strands from the trimer of hairpins and reduced helicity for the N-helices, with resulting larger average distances between the membranes, and impaired fusion catalysis. The G1E model shows binding of the FP to the C-terminal strands, which results in more distant membrane apposition and weaker binding of the FP to the target membrane, and consequent impaired fusion catalysis. The displayed G1E structure is in equilibrium with the WT structure, like in Figure 2.

consequent much greater level of aqueous exposure of the bundle, as supported by the much larger $\langle D_{\%}\rangle$ of the 22−69 fragment for I173E versus WT, e.g., $\langle D_{\%}\rangle_{22-38}$ values of 35% versus 17%, $\langle D_{\%}\rangle_{39-52}$ values of 47% versus 3%, and $\langle D_{\%}\rangle_{53-69}$ values of 18% versus 6%. SE hairpin turns and C-terminal strands are on the exterior of the WT structure and exhibit significant $\langle D_{\%}\rangle$ values, but even larger $\langle D_{\%}\rangle$ values for I173E in these segments support strand dissociation and SE destabilization. For the same peptide in 100−115 and 151−191, the $\langle D_{\%}\rangle$ values are always larger for I173E than for WT, e.g., 60% versus 50% for the 172−178 peptide that contains the mutation site. The model in Figure 8 supports the idea that highly impaired fusion for I173E is due to a greater intermembrane distance that results from a more flexible SE hairpin.

Figure 8 (right) displays a model for G1E-HA2 with a I173E-like SE structure with a dissociated C-terminal strand bound to unfolded FP. This structure is in equilibrium with the WT structure, like in Figure 2. G1E fusion is consequently impaired both by membrane apposition at a greater distance and by weakened interaction of the FP with the target membrane. G1E may destabilize the membrane-interacting helical hairpin FP structure by reduction of the N-terminal $NH_3^+$ charge/12−22 helix dipole interaction.[43] FP/SE strand binding helps explain the G1E destabilization of the SE, where the latter observation was unanticipated because the trimer-of-hairpins structure of the SE is thermostable in the absence of the FP.[14] FP/SE binding in Figure 8 is consistent with a decreased level of aqueous exposure of G1E FP; e.g., $\langle D_{\%}\rangle_{10-21}$ = 45% for G1E versus 54% for WT, and $\langle D_{\%}\rangle_{12-22}$ = 49% for G1E versus 63% for I173E. G1E likely has the least thermostable FP and without SE binding would exhibit higher rather than lower levels of aqueous exposure and exchange. Partial dissociation of the C-terminal strand for G1E is consistent with $\langle D_{\%}\rangle$ values for the 151−191 region that are intermediate between the smaller WT and larger I173E values. Distinct G1E SE states similar to either WT or I173E structures are also evidenced by the bimodal behavior for the 39−52 fragment, with one distribution of peaks in a $m/z$ range similar to that of WT and the other in a $m/z$ range similar to that of I173E (Figure 5). For $t_{HDX}$ = 120 min, there are approximately equal sums of G1E peak intensities in the two ranges, and the calculated $D_{\%}$ values of 16% and 63% are similar to the values of 6% and 54% for WT and I173E, respectively. Table S3 lists the $D_{\%}$ values for the 39−52 fragment for all $t_{HDX}$ values. There are similar $\langle D_{\%}\rangle$ values for G1E and WT for peptides in the 22−38, 53−150, and 192−217 regions.



DOI: 10.1021/acs.biochem.8b01272
*Biochemistry* 2019, 58, 2432−2446

**Integration with Previous Studies.** The high $T_m$ of 91 °C of WT-HA2 correlates with the highly ordered structural model in Figure 8. The thermostability and rigidity of WT-HA2 are needed for the membrane apposition function of HA2 in fusion. The lower $T_m$ values of 79 °C for I173E and 75 °C for G1E correlate with the loss of SE structure and the consequent increased intermembrane distance and impaired fusion (Figure 8).[15]

The FP and TM in Figure 8 are displayed with membrane-interfacial and traversal locations, respectively, that correlate with peptides with a $\langle D_{\%} \rangle$ value of >35% in the 1−21 region and a $\langle D_{\%} \rangle$ value of <3% in the 192−205 region. The low $\langle D_{\%} \rangle$ values of TM are consistent with either the monomer or the oligomer TM that traverses the membrane. The monomer TM is consistent with the low degree of sequence conservation in this domain among HA subtypes and with robust HA-cell/RBC fusion after substitution of the native TM and endodomain sequences with those of an unrelated protein.[4,39] However, cryo-electron microscopy of the HA2/HA1 initial trimer complex in a detergent was interpreted to support a trimeric TM bundle.[36] We note that fluorescence and SDS−PAGE data for HA2 TM peptides support a fraction of oligomeric peptides.[37,44]

The $\langle D_{\%} \rangle$ values of 63% for the 1−8 fragment and 54% for the 10−21 fragment from the FP of HA2 are comparable with the $\langle D_{\%} \rangle$ value of 57% of the 206−217 fragment that includes part of the likely unstructured and aqueous exposed $HA2_{212-221}$ endodomain. Thus, the FP $\langle D_{\%} \rangle$ could be consistent with unfolded FP in aqueous solution. However, we consider this scenario unlikely because of the stability of the FP helical hairpin in detergent and membrane and the hydrophobic-effect free energy penalty associated with aqueous solubilization.[24,27,45] The larger $\langle D_{\%} \rangle$ values of FP in HA2 versus FHA2 are completely inconsistent with a FP/TM complex, but we note that earlier fluorescence, EPR, and calorimetric data were interpreted to support weak association in the membrane between a peptide containing the TM sequence and a peptide containing the FP sequence.[37,46] By contrast, there was no close contact between the FP and TM domains of a 194-residue FP +SE+TM HIV gp41 fusion protein construct.[47] HIV gp41 is nonhomologous with HA2, but the SE's of the two proteins both adopt trimer-of-hairpins structures.[40,48−50] Finally, we note that although the preponderance of simulations and experimental data support a membrane-interfacial location for the FP in the absence of the rest of HA2, there are some simulations and experimental data that support membrane traversal for the isolated FP.[24,51−55]

The models in Figure 8 and Figure S2 have local positive membrane curvature to achieve interfacial locations for the FP and the N-terminus of the TM. HA2-stabilized curvature could be important for fusion catalysis, as there are likely membrane intermediates during fusion with local curvature.[1,56] Earlier studies have provided experimental data that evidence stabilization of local membrane curvature by viral fusion peptides.[57−60]

The $D_{\%}$ data from this study are compared to those of an earlier study in which the $HA2_{1-175}$/HA1 complex that lacked the TM and endodomain was incubated in a pH 4.9 solution without detergent for 3 h, neutralized, and subjected to a protocol similar to that described in the study presented here.[34] The earlier protocol included incubation in 85% $D_2O$ for $t_{HDX}$ = 0.05, 1, 30, or 1200 min, acidification, pepsin digestion, and mass spectrometric analysis of the peptide products. Direct comparison can be made between the $D_{\%}$ for $t_{HDX}$ = 1 and 30 min, which are common to both studies. Comparison is made using our data for FHA2 ≡ $HA2_{1-185}$, as this construct is closest to the $HA2_{1-175}$ subunit of the complex with HA1. There are minor differences in how $D_{\%}$ was calculated in the two studies. As noted earlier, our $D_{\%}$ values do not account for back-exchange and might therefore be reduced by ∼0.8 relative to the earlier study that appeared to account for back-exchange. For both studies, peptides in the 53−99 region exhibit $D_{\%}$ values of <5%, which is consistent with the interior location of the 38−105 helices of the trimer-of-hairpins structure. For both studies, peptides from the 99−171 region exhibit larger $D_{\%}$ values, which correlates with the exterior location of most of this region in the structure. However, the $D_{\%}$ values for the study presented here are much lower than those from the previous study, even with a 0.8 multiplication of the previous values. Figure S3 provides some examples of this trend that holds for the 22−52 and 99−171 regions. For example, comparison of the 22−38 region for FHA2 versus $HA2_{1-175}$/HA1 shows $D_{\%}$ values of 14% and 75% for $t_{HDX}$ = 1 min and $D_{\%}$ values of 17% and 85% for $t_{HDX}$ = 30 min, respectively. For the 39−52 fragment, $D_{\%}$ = 2% and 40% for $t_{HDX}$ = 1 min and $D_{\%}$ = 5% and 55% for $t_{HDX}$ = 30 min, respectively. For the 110−115 peptide at either $t_{HDX}$, $D_{\%}$ = 26% and 100%, respectively. For the 151−167 peptide, $D_{\%}$ = 35% and 80% for $t_{HDX}$ = 1 min and $D_{\%}$ = 37% and 100% for $t_{HDX}$ = 30 min, respectively. Another difference is that peptides from the FP were straightforwardly analyzed in the study presented here with HA2-only constructs but not in the earlier study with low-pH incubation of the $HA2_{1-175}$/HA1 complex because of significant broadening of the envelopes of peaks. Such broadening was not observed for the complex that had not undergone the incubation and consequent large-scale structural rearrangement. One experimental difference between the study presented here and the earlier study is the presence and absence of detergent, respectively. HA2 constructs form aggregates in the absence of detergent via the exposed FP's. Detergent is also important for FHA2 folding as evidenced by circular dichroism $\theta_{222}$ values that correlate with 65% and 25% helicity in the presence and absence of detergent, respectively.[15,21] The 65% helicity in detergent is consistent with folded protein as it matches the percent helicity calculated using the numbers of helical residues in the trimer-of-hairpins SE structure and in the helical hairpin FP structure in detergent. The envelope broadening of peptides from the FP and the larger $D_{\%}$ of the earlier study may therefore reflect $HA2_{1-175}$ proteins that are aggregated and less folded than the HA2 constructs in detergent in the study presented here.

We also compare the $D_{\%}$ of the FP region of the study presented here with earlier NMR-measured HDX rates for $HA2_{1-23}$ in detergent.[24] Residues 2−6, 12−17, and 20−23 exhibit rates of >0.1 $s^{-1}$ and would be completely exchanged even for the shortest $t_{HDX}$ of 1 min in the study presented here. For $t_{HDX}$ = 1 min, the 1−9 peptide exhibits a $D_{\%}$ of 20% for FHA2 versus a $D_{\%}$ of 45% for HA2 and 10−21 exhibits a $D_{\%}$ of 35% for FHA2 versus a $D_{\%}$ of 44% for HA2. For a model in which FP residues 2−6, 12−17, and 20−23 completely exchange and other residues do not exchange, the calculated $D_{\%}$ = 63% for residues 1−9 and $D_{\%}$ = 73% for residues 10−21. The FP therefore exhibits greater protection in FHA2 and HA2 than in $HA2_{1-23}$.

**Dependence of $D_{\%}$ on $t_{HDX}$.** For the study presented here, peptides from the exterior of the SE often exhibit significant $D_{\%}$ for $t_{HDX}$ = 1 min and then small increases in $D_{\%}$ for larger $t_{HDX}$ values up to the maximum of 2 h. $D_{\%}$ is a measure of aqueous exposure, as supported by negligible exchange of the N-helix in



DOI: 10.1021/acs.biochem.8b01272
Biochemistry 2019, 58, 2432−2446

WT-FHA2 and HA2, and negligible exchange of TM in all HA2 proteins. Peptides from structured regions on the protein exterior have some residues facing outward with aqueous exposure and some facing inward without exposure. Even modest exposure results in complete exchange at $t_{HDX}$ = 1 min, as supported by the calculated complete exchange in 1 min for the slowest NMR-measured exchange rate for $HA2_{1-23}$ described above. Thus, the $D_{\%}$ value at $t_{HDX}$ = 1 min for peptides from the outside of the HA2 SE likely reflects their fraction of aqueous-exposed residues. The small increases in $D_{\%}$ with larger $t_{HDX}$ values for the WT proteins likely reflect their structural stability and small unfolded population, which is consistent with their $T_m$ values of >85 °C. The bimodal data for G1E-$HA2_{39-52}$ are also consistent with this model, with one population with a low level of exchange from protein that remains folded and a second population with a high level of exchange from protein that has transiently unfolded. The latter fractional population increases with $t_{HDX}$. Similar trends of $D_{\%}$ versus $t_{HDX}$ over the range from 1 min to 2 h has also been observed for other proteins.[33]

## SUMMARY

HDX-MS has been applied to subunit 2 of the influenza virus hemagglutinin protein that mediates fusion between the virus and endosome membranes. A high level of aqueous exposure of the fusion peptide and a high level of aqueous protection of the transmembrane region are consistent with separate domains that have respective membrane-interfacial and traversal locations. The HDX-MS data are also consistent with a trimer-of-hairpins structure for the soluble ectodomain. A high level of aqueous protection of the 22−38 peptide supports a well-structured segment and is consistent with retention of the 23−35 antiparallel $\beta$ sheet found in the initial HA2/HA1 complex. The $\beta$ sheet provides a semirigid connection between the fusion peptide and soluble ectodomain and aids close apposition of the two membranes prior to fusion. HDX-MS was also performed on the G1E and I173E mutants that result in highly impaired fusion. I173E shows a much higher level of aqueous exposure versus WT of the 22−69 and 150−191 regions, which correlates with dissociation of the C-terminal strands of the trimer of hairpins. G1E has a level of aqueous exposure of these regions intermediate between those of WT and I173E as well as an increased level of protection of the fusion peptide. These data are consistent with binding of the G1E fusion peptide to the dissociated C-terminal strands. The HDX-MS data support a model in which a reduced level of fusion by the mutants is due to the larger distance between the apposed membranes and for G1E also the loss of the contact of the fusion peptide with the target membrane.

## ASSOCIATED CONTENT

### Supporting Information

The Supporting Information is available free of charge on the ACS Publications website at DOI: 10.1021/acs.biochem.8b01272.

Sequence coverages of the peptides observed by mass spectrometry, tables of values of $D_{\%}$ versus $t_{HDX}$ for all observed peptides, HA2 structures in a single membrane, and a plot comparing $D_{\%}$ data from the study presented here and a previous study (PDF)

### Accession Codes

HA2, UniProtKB entry P03437.

## AUTHOR INFORMATION


### Corresponding Author

*E-mail: weliky@chemistry.msu.edu. Phone: 517-353-1177. Fax: 517-355-9715.

### ORCID

David P. Weliky: 0000-0002-2765-5950



### Funding

This work was supported by National Institutes of Health Grant R01 AI047153.

### Notes

The authors declare no competing financial interest.

## ACKNOWLEDGMENTS

The authors acknowledge advice and assistance from Drs. Dan Jones, Tony Shilmiller, Sundari Chodavarapu, and Tom Carter. The HDX-MS experiments were performed in the Michigan State University Mass Spectrometry facility.


## ABBREVIATIONS

ACN, acetonitrile; CD, circular dichroism; DM, decyl maltoside; FA, formic acid; FP, fusion peptide; HA, hemagglutinin; HDX, hydrogen−deuterium exchange; LB, Luria-Bertani; LC, liquid chromatography; MS, mass spectrometry; PBS, phosphate-buffered saline; PDB, Protein Data Bank; RBC, red blood cell; SDS−PAGE, sodium dodecyl sulfate−polyacrylamide gel electrophoresis; SE, soluble ectodomain; SHB, six-helix bundle; TM, transmembrane domain; WT, wild-type.

## REFERENCES


(1) White, J. M., Delos, S. E., Brecher, M., and Schornberg, K. (2008) Structures and mechanisms of viral membrane fusion proteins: Multiple variations on a common theme. *Crit. Rev. Biochem. Mol. Biol. 43*, 189−219.

(2) Harrison, S. C. (2015) Viral membrane fusion. *Virology 479*, 498−507.

(3) Boonstra, S., Blijleven, J. S., Roos, W. H., Onck, P. R., van der Giessen, E., and van Oijen, A. M. (2018) Hemagglutinin-mediated membrane fusion: A biophysical perspective. *Annu. Rev. Biophys. 47*, 153−173.

(4) Nobusawa, E., Aoyama, T., Kato, H., Suzuki, Y., Tateno, Y., and Nakajima, K. (1991) Comparison of complete amino acid sequences and receptor binding properties among 13 serotypes of hemagglutinins of influenza A viruses. *Virology 182*, 475−485.

(5) Wilson, I. A., Skehel, J. J., and Wiley, D. C. (1981) Structure of the haemagglutinin membrane glycoprotein of influenza virus at 3 A resolution. *Nature 289*, 366−373.

(6) Ekiert, D. C., Kashyap, A. K., Steel, J., Rubrum, A., Bhabha, G., Khayat, R., Lee, J. H., Dillon, M. A., O'Neil, R. E., Faynboym, A. M., Horowitz, M., Horowitz, L., Ward, A. B., Palese, P., Webby, R., Lerner, R. A., Bhatt, R. R., and Wilson, I. A. (2012) Cross-neutralization of influenza A viruses mediated by a single antibody loop. *Nature 489*, 526−532.

(7) Lakadamyali, M., Rust, M. J., Babcock, H. P., and Zhuang, X. W. (2003) Visualizing infection of individual influenza viruses. *Proc. Natl. Acad. Sci. U. S. A. 100*, 9280−9285.

(8) Chen, J., Skehel, J. J., and Wiley, D. C. (1999) N- and C-terminal residues combine in the fusion-pH influenza hemagglutinin $HA_2$ subunit to form an N cap that terminates the triple-stranded coiled coil. *Proc. Natl. Acad. Sci. U. S. A. 96*, 8967−8972.

(9) Blijleven, J. S., Boonstra, S., Onck, P. R., van der Giessen, E., and van Oijen, A. M. (2016) Mechanisms of influenza viral membrane fusion. *Semin. Cell Dev. Biol. 60*, 78−88.

(10) Chernomordik, L. V., Frolov, V. A., Leikina, E., Bronk, P., and Zimmerberg, J. (1998) The pathway of membrane fusion catalyzed by




DOI: 10.1021/acs.biochem.8b01272
*Biochemistry* 2019, 58, 2432−2446

influenza hemagglutinin: Restriction of lipids, hemifusion, and lipidic fusion pore formation. *J. Cell Biol. 140*, 1369−1382.
(11) Qiao, H., Armstrong, R. T., Melikyan, G. B., Cohen, F. S., and White, J. M. (1999) A specific point mutant at position 1 of the influenza hemagglutinin fusion peptide displays a hemifusion phenotype. *Mol. Biol. Cell 10*, 2759−2769.
(12) Cho, K. J., Lee, J.-H., Hong, K. W., Kim, S.-H., Park, Y., Lee, J. Y., Kang, S., Kim, S., Yang, J. H., Kim, E.-K., Seok, J. H., Unzai, S., Park, S. Y., Saelens, X., Kim, C.-J., Lee, J.-Y., Kang, C., Oh, H.-B., Chung, M. S., and Kim, K. H. (2013) Insight into structural diversity of influenza virus haemagglutinin. *J. Gen. Virol. 94*, 1712−1722.
(13) Xiong, X., Corti, D., Liu, J., Pinna, D., Foglierini, M., Calder, L. J., Martin, S. R., Lin, Y. P., Walker, P. A., Collins, P. J., Monne, I., Suguitan, A. L., Jr., Santos, C., Temperton, N. J., Subbarao, K., Lanzavecchia, A., Gamblin, S. J., and Skehel, J. J. (2015) Structures of complexes formed by H5 influenza hemagglutinin with a potent broadly neutralizing human monoclonal antibody. *Proc. Natl. Acad. Sci. U. S. A. 112*, 9430−9435.
(14) Ratnayake, P. U., Prabodha Ekanayaka, E. A., Komanduru, S. S., and Weliky, D. P. (2016) Full-length trimeric influenza virus hemagglutinin II membrane fusion protein and shorter constructs lacking the fusion peptide or transmembrane domain: Hyperthermostability of the full-length protein and the soluble ectodomain and fusion peptide make significant contributions to fusion of membrane vesicles. *Protein Expression Purif. 117*, 6−16.
(15) Ranaweera, A., Ratnayake, P. U., and Weliky, D. P. (2018) The stabilities of the soluble ectodomain and fusion peptide hairpins of the Influenza virus hemagglutinin subunit II protein are positively correlated with membrane fusion. *Biochemistry 57*, 5480−5493.
(16) Chlanda, P., Mekhedov, E., Waters, H., Schwartz, C. L., Fischer, E. R., Ryham, R. J., Cohen, F. S., Blank, P. S., and Zimmerberg, J. (2016) The hemifusion structure induced by influenza virus haemagglutinin is determined by physical properties of the target membranes. *Nat. Microbiol. 1*, 16050.
(17) Gui, L., Ebner, J. L., Mileant, A., Williams, J. A., and Lee, K. K. (2016) Visualization and sequencing of membrane remodeling leading to influenza virus fusion. *J. Virol. 90*, 6948−6962.
(18) Das, D. K., Govindan, R., Nikic-Spiegel, I., Krammer, F., Lemke, E. A., and Munro, J. B. (2018) Direct visualization of the conformational dynamics of single influenza hemagglutinin trimers. *Cell 174*, 926−937.
(19) Eddy, N. R., and Onuchic, J. N. (2018) Rotation-activated and cooperative zipping characterize class I viral fusion protein dynamics. *Biophys. J. 114*, 1878−1888.
(20) Leikina, E., LeDuc, D. L., Macosko, J. C., Epand, R., Epand, R., Shin, Y. K., and Chernomordik, L. V. (2001) The 1−127 HA2 construct of influenza virus hemagglutinin induces cell-cell hemifusion. *Biochemistry 40*, 8378−8386.
(21) Kim, C. S., Epand, R. F., Leikina, E., Epand, R. M., and Chernomordik, L. V. (2011) The final conformation of the complete ectodomain of the HA2 subunit of Influenza Hemagglutinin can by itself drive low pH-dependent fusion. *J. Biol. Chem. 286*, 13226−13234.
(22) Carr, C. M., and Kim, P. S. (1993) A spring-loaded mechanism for the conformational change of influenza hemagglutinin. *Cell 73*, 823−832.
(23) Durrer, P., Galli, C., Hoenke, S., Corti, C., Gluck, R., Vorherr, T., and Brunner, J. (1996) H+-induced membrane insertion of influenza virus hemagglutinin involves the HA2 amino-terminal fusion peptide but not the coiled coil region. *J. Biol. Chem. 271*, 13417−13421.
(24) Lorieau, J. L., Louis, J. M., and Bax, A. (2010) The complete influenza hemagglutinin fusion domain adopts a tight helical hairpin arrangement at the lipid:water interface. *Proc. Natl. Acad. Sci. U. S. A. 107*, 11341−11346.
(25) Ghosh, U., Xie, L., and Weliky, D. P. (2013) Detection of closed influenza virus hemagglutinin fusion peptide structures in membranes by backbone $^{13}CO$-$^{15}N$ rotational-echo double-resonance solid-state NMR. *J. Biomol. NMR 55*, 139−146.
(26) Du, T. P., Jiang, L., and Liu, M. L. (2014) NMR structures of fusion peptide from influenza hemagglutinin H3 subtype and its mutants. *J. Pept. Sci. 20*, 292−297.
(27) Ghosh, U., Xie, L., Jia, L. H., Liang, S., and Weliky, D. P. (2015) Closed and semiclosed interhelical structures in membrane vs closed and open structures in detergent for the Influenza Virus hemagglutinin fusion peptide and correlation of hydrophobic surface area with fusion catalysis. *J. Am. Chem. Soc. 137*, 7548−7551.
(28) Macosko, J. C., Kim, C. H., and Shin, Y. K. (1997) The membrane topology of the fusion peptide region of influenza hemagglutinin determined by spin-labeling EPR. *J. Mol. Biol. 267*, 1139−1148.
(29) Marcsisin, S. R., and Engen, J. R. (2010) Hydrogen exchange mass spectrometry: what is it and what can it tell us? *Anal. Bioanal. Chem. 397*, 967−972.
(30) Pirrone, G. F., Iacob, R. E., and Engen, J. R. (2015) Applications of hydrogen/deuterium exchange MS from 2012 to 2014. *Anal. Chem. 87*, 99−118.
(31) Koshy, S. S., Eyles, S. J., Weis, R. M., and Thompson, L. K. (2013) Hydrogen exchange mass spectrometry of functional membrane-bound chemotaxis receptor complexes. *Biochemistry 52*, 8833−8842.
(32) Koshy, S. S., Li, X., Eyles, S. J., Weis, R. M., and Thompson, L. K. (2014) Hydrogen exchange differences between chemoreceptor signaling complexes localize to functionally important subdomains. *Biochemistry 53*, 7755−7764.
(33) Chodavarapu, S., Jones, A. D., Feig, M., and Kaguni, J. M. (2016) DnaC traps DnaB as an open ring and remodels the domain that binds primase. *Nucleic Acids Res. 44*, 210−220.
(34) Garcia, N. K., Guttman, M., Ebner, J. L., and Lee, K. K. (2015) Dynamic changes during acid-Induced activation of influenza hemagglutinin. *Structure 23*, 665−676.
(35) Tamm, L. K. (2003) Hypothesis: spring-loaded boomerang mechanism of influenza hemagglutinin-mediated membrane fusion. *Biochim. Biophys. Acta, Biomembr. 1614*, 14−23.
(36) Benton, D. J., Nans, A., Calder, L. J., Turner, J., Neu, U., Lin, Y. P., Ketelaars, E., Kallewaard, N. L., Corti, D., Lanzavecchia, A., Gamblin, S. J., Rosenthal, P. B., and Skehel, J. J. (2018) Influenza hemagglutinin membrane anchor. *Proc. Natl. Acad. Sci. U. S. A. 115*, 10112−10117.
(37) Chang, D. K., Cheng, S. F., Kantchev, E. A. B., Lin, C. H., and Liu, Y. T. (2008) Membrane interaction and structure of the transmembrane domain of influenza hemagglutinin and its fusion peptide complex. *BMC Biol. 6*, 2.
(38) Armstrong, R. T., Kushnir, A. S., and White, J. M. (2000) The transmembrane domain of influenza hemagglutinin exhibits a stringent length requirement to support the hemifusion to fusion transition. *J. Cell Biol. 151*, 425−437.
(39) Melikyan, G. B., Lin, S. S., Roth, M. G., and Cohen, F. S. (1999) Amino acid sequence requirements of the transmembrane and cytoplasmic domains of influenza virus hemagglutinin for viable membrane fusion. *Mol. Biol. Cell 10*, 1821−1836.
(40) Liang, S., Ratnayake, P. U., Keinath, C., Jia, L., Wolfe, R., Ranaweera, A., and Weliky, D. P. (2018) Efficient fusion at neutral pH by Human Immunodeficiency Virus gp41 trimers containing the fusion peptide and transmembrane domains. *Biochemistry 57*, 1219−1235.
(41) Weis, D. D., Engen, J. R., and Kass, I. J. (2006) Semi-automated data processing of hydrogen exchange mass spectra using HX-Express. *J. Am. Soc. Mass Spectrom. 17*, 1700−1703.
(42) Markosyan, R. M., Cohen, F. S., and Melikyan, G. B. (2000) The lipid-anchored ectodomain of influenza virus hemagglutinin (GPI-HA) is capable of inducing nonenlarging fusion pores. *Mol. Biol. Cell 11*, 1143−1152.
(43) Lorieau, J. L., Louis, J. M., and Bax, A. (2011) Helical hairpin structure of Influenza Hemagglutinin fusion peptide stabilized by charge-dipole interactions between the N-terminal amino group and the second helix. *J. Am. Chem. Soc. 133*, 2824−2827.
(44) Tatulian, S. A., and Tamm, L. K. (2000) Secondary structure, orientation, oligomerization, and lipid interactions of the transmembrane domain of influenza hemagglutinin. *Biochemistry 39*, 496−507.


DOI: 10.1021/acs.biochem.8b01272
*Biochemistry* 2019, 58, 2432−2446

(45) Han, X., and Tamm, L. K. (2000) A host-guest system to study structure-function relationships of membrane fusion peptides. *Proc. Natl. Acad. Sci. U. S. A. 97*, 13097−13102.
(46) Lai, A. L., and Freed, J. H. (2015) The interaction between Influenza HA fusion peptide and transmembrane domain affects membrane structure. *Biophys. J. 109*, 2523−2536.
(47) Lakomek, N. A., Kaufman, J. D., Stahl, S. J., Louis, J. M., Grishaev, A., Wingfield, P. T., and Bax, A. (2013) Internal dynamics of the homotrimeric HIV-1 viral coat protein gp41 on multiple time scales. *Angew. Chem., Int. Ed. 52*, 3911−3915.
(48) Caffrey, M., Cai, M., Kaufman, J., Stahl, S. J., Wingfield, P. T., Covell, D. G., Gronenborn, A. M., and Clore, G. M. (1998) Three-dimensional solution structure of the 44 kDa ectodomain of SIV gp41. *EMBO J. 17*, 4572−4584.
(49) Yang, Z. N., Mueser, T. C., Kaufman, J., Stahl, S. J., Wingfield, P. T., and Hyde, C. C. (1999) The crystal structure of the SIV gp41 ectodomain at 1.47 A resolution. *J. Struct. Biol. 126*, 131−144.
(50) Sackett, K., Nethercott, M. J., Epand, R. F., Epand, R. M., Kindra, D. R., Shai, Y., and Weliky, D. P. (2010) Comparative analysis of membrane-associated fusion peptide secondary structure and lipid mixing function of HIV gp41 constructs that model the early pre-hairpin intermediate and final hairpin conformations. *J. Mol. Biol. 397*, 301−315.
(51) Panahi, A., and Feig, M. (2010) Conformational sampling of Influenza fusion peptide in membrane bilayers as a function of termini and protonation states. *J. Phys. Chem. B 114*, 1407−1416.
(52) Baylon, J. L., and Tajkhorshid, E. (2015) Capturing spontaneous membrane insertion of the Influenza virus Hemagglutinin fusion peptide. *J. Phys. Chem. B 119*, 7882−7893.
(53) Jia, L. H., Liang, S., Sackett, K., Xie, L., Ghosh, U., and Weliky, D. P. (2015) REDOR solid-state NMR as a probe of the membrane locations of membrane-associated peptides and proteins. *J. Magn. Reson. 253*, 154−165.
(54) Victor, B. L., Lousa, D., Antunes, J. M., and Soares, C. M. (2015) Self-assembly molecular dynamics simulations shed light into the interaction of the influenza fusion peptide with a membrane bilayer. *J. Chem. Inf. Model. 55*, 795−805.
(55) Worch, R., Dudek, A., Krupa, J., Szymaniec, A., and Setny, P. (2018) Charged N-terminus of influenza fusion peptide facilitates membrane fusion. *Int. J. Mol. Sci. 19*, 578.
(56) Kuzmin, P. I., Zimmerberg, J., Chizmadzhev, Y. A., and Cohen, F. S. (2001) A quantitative model for membrane fusion based on low-energy intermediates. *Proc. Natl. Acad. Sci. U. S. A. 98*, 7235−7240.
(57) Epand, R. M., Epand, R. F., Martin, I., and Ruysschaert, J. M. (2001) Membrane interactions of mutated forms of the influenza fusion peptide. *Biochemistry 40*, 8800−8807.
(58) Gabrys, C. M., Yang, R., Wasniewski, C. M., Yang, J., Canlas, C. G., Qiang, W., Sun, Y., and Weliky, D. P. (2010) Nuclear magnetic resonance evidence for retention of a lamellar membrane phase with curvature in the presence of large quantities of the HIV fusion peptide. *Biochim. Biophys. Acta, Biomembr. 1798*, 194−201.
(59) Tristram-Nagle, S., Chan, R., Kooijman, E., Uppamoochikkal, P., Qiang, W., Weliky, D. P., and Nagle, J. F. (2010) HIV fusion peptide penetrates, disorders, and softens T-cell membrane mimics. *J. Mol. Biol. 402*, 139−153.
(60) Yao, H. W., and Hong, M. (2013) Membrane-dependent conformation, dynamics, and lipid Interactions of the fusion peptide of the paramyxovirus PIV5 from solid-state NMR. *J. Mol. Biol. 425*, 563−576.


DOI: 10.1021/acs.biochem.8b01272
*Biochemistry* 2019, 58, 2432−2446

**Supporting Information for Publication**

# Hydrogen-deuterium exchange supports independent membrane-interfacial fusion peptide and transmembrane domains in subunit 2 of influenza virus hemagglutinin protein, a structured and aqueous-protected connection between the fusion peptide and soluble ectodomain, and the importance of membrane apposition by the trimer-of-hairpins structure

Ahinsa Ranaweera, Punsisi U. Ratnayake, E. A. Prabodha Ekanayaka, Robin DeClercq, and David P. Weliky*

Department of Chemistry, Michigan State University, East Lansing, MI 48824 USA

**Figure S1.** Sequences with peptides observed by mass spectrometry underlined with domains colored: fusion peptide (FP), pink; soluble ectodomain (SE), blue; transmembrane domain (TM), green; and endodomain, orange. The non-native C-terminal regions are in black.

**FHA2**

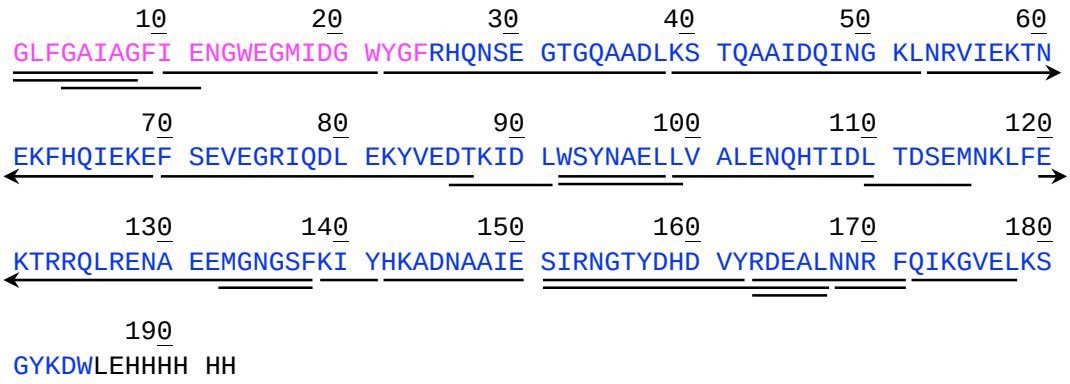


**SHA2_TM**

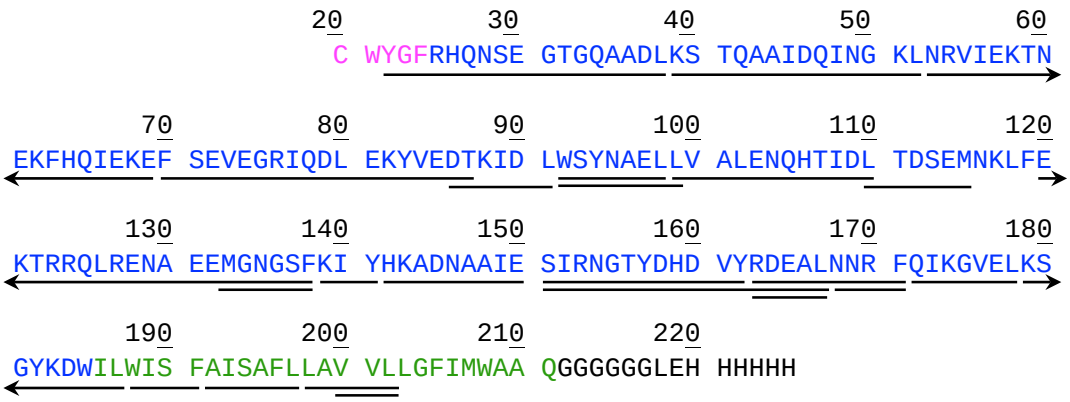

## HA2

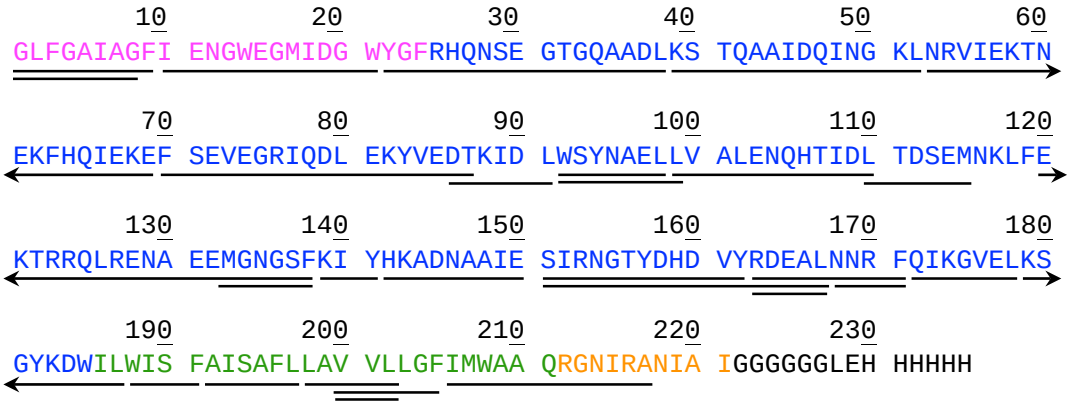


## G1E-HA2

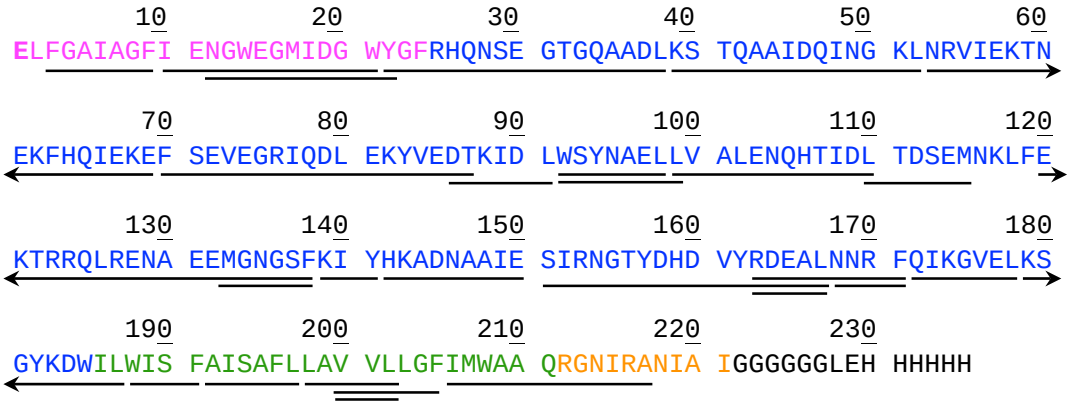


## I173E-HA2

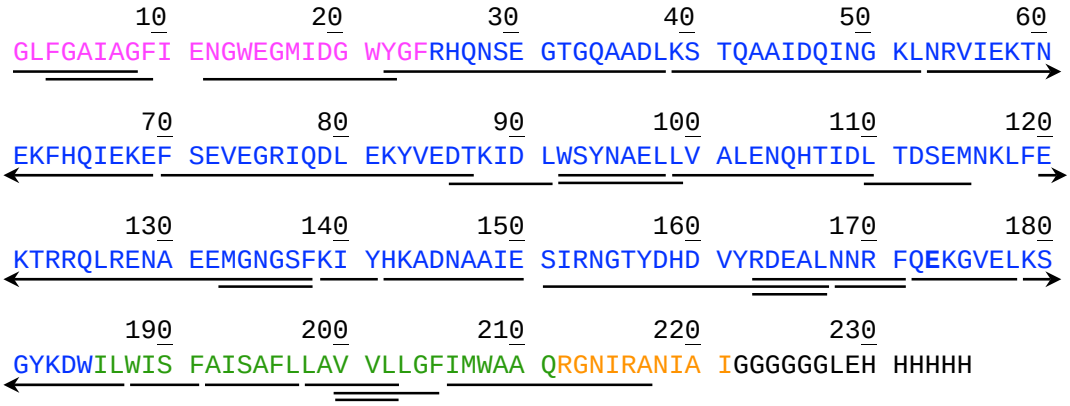

**Tables S1**. Percent deuterium incorporation vs. HDX time for peptides from FHA2, SHA2_TM, and HA2. Each value is the average of triplicate measurements, and the standard deviation is given in parentheses.

| HDX time/min | Deuterium Incorporation (%) (1-8) | |
|---|---|---|
| | FHA2 | HA2 |
| 1 | 22.86 (0.62) | 47.00 (1.21) |
| 5 | 34.86 (1.03) | 63.05 (0.73) |
| 30 | 48.77 (1.19) | 66.38 (1.72) |
| 60 | 56.21 (1.71) | 68.90 (1.21) |
| 120 | 61.71 (1.62) | 69.76 (0.46) |

| HDX time/min | Deuterium Incorporation (%) (1-9) | |
|---|---|---|
| | FHA2 | HA2 |
| 1 | 19.79 (0.85) | 45.31 (2.21) |
| 5 | 36.75 (0.43) | 61.88 (2.12) |
| 30 | 55.50 (0.82) | 67.13 (2.29) |
| 60 | 56.25 (0.00) | 69.92 (2.74) |
| 120 | 65.83 (1.57) | 70.93 (0.26) |

| HDX time/min | Deuterium Incorporation (%) (10-21) | |
|---|---|---|
| | FHA2 | HA2 |
| 1 | 34.58 (2.78) | 43.58 (0.18) |
| 5 | 37.27 (0.77) | 46.09 (0.00) |
| 30 | 39.27 (0.68) | 57.05 (1.09) |
| 60 | 39.91 (1.02) | 57.07 (1.09) |
| 120 | 41.21 (1.28) | 65.59 (0.06) |

| HDX time/min | Deuterium Incorporation (%) (4-11) FHA2 |
|---|---|
| 1 | 20.86 (0.51) |
| 5 | 28.33 (0.21) |
| 30 | 37.10 (2.06) |
| 60 | 42.05 (3.13) |
| 120 | 45.00 (0.01) |

| HDX time/min | Deuterium Incorporation (%) (22-38) | | |
|---|---|---|---|
| | FHA2 | SHA2_TM | HA2 |
| 1 | 14.40 (2.38) | 8.69 (0.00) | 12.83 (2.02) |
| 5 | 15.73 (1.15) | 10.79 (0.85) | 15.81 (0.50) |
| 30 | 16.60 (0.07) | 13.33 (2.17) | 17.60 (1.87) |
| 60 | 18.25 (0.92) | 15.63 (1.32) | 19.69 (1.77) |
| 120 | 20.98 (1.16) | 17.19 (0.60) | 21.21 (0.22) |

| HDX time/min | Deuterium Incorporation (%) (39-52) | | |
|---|---|---|---|
| | FHA2 | SHA2_TM | HA2 |
| 1 | 1.95 (0.22) | 6.18 (0.32) | 0.74 (0.24) |
| 5 | 3.90 (1.35) | 7.08 (0.25) | 1.59 (0.51) |
| 30 | 5.28 (0.58) | 7.61 (0.27) | 3.49 (0.85) |
| 60 | 5.79 (0.54) | 7.97 (0.40) | 4.64 (0.45) |
| 120 | 6.77 (0.75) | 11.97 (0.09) | 5.85 (0.23) |

| HDX time/min | Deuterium Incorporation (%) (53-69) | | |
|---|---|---|---|
| | FHA2 | SHA2_TM | HA2 |
| 1 | 1.63 (1.23) | 4.25 (0.68) | 4.68 (0.77) |
| 5 | 2.91 (0.49) | 4.79 (0.91) | 4.63 (0.18) |
| 30 | 3.72 (0.31) | 5.04 (0.84) | 5.99 (0.61) |
| 60 | 4.00 (0.35) | 5.63 (0.31) | 6.00 (0.35) |
| 120 | 4.41 (0.93) | 5.53 (0.04) | 6.21 (0.44) |

| HDX time/min | Deuterium Incorporation (%) (70-87) | | |
|---|---|---|---|
| | FHA2 | SHA2_TM | HA2 |
| 1 | 0.09 (0.12) | 2.21 (0.04) | 1.68 (0.21) |
| 5 | 0.29 (0.41) | 3.09 (029) | 1.68 (0.04) |
| 30 | 1.26 (1.54) | 3.44 (0.04) | 2.00 (0.17) |
| 60 | 1.47 (0.99) | 3.97 (0.37) | 2.21 (0.04) |
| 120 | 5.18 (3.41) | 4.65 (0.58) | 2.50 (0.04) |

| HDX time/min | Deuterium Incorporation (%) (86-91) | | |
|---|---|---|---|
| | FHA2 | SHA2_TM | HA2 |
| 1 | 1.00 (1.56) | 0.20 (0.28) | 2.07 (1.33) |
| 5 | 0.40 (0.28) | 2.70 (2.40) | 1.93 (0.41) |
| 30 | 0.47 (0.23) | 5.00 (0.84) | 1.50 (0.14) |
| 60 | 1.20 (1.38) | 5.70 (0.98) | 3.53 (1.89) |
| 120 | 6.00 (0.20) | 7.20 (0.20) | 6.07 (1.33) |

| HDX time/min | Deuterium Incorporation (%) (92-98) | | |
|---|---|---|---|
| | FHA2 | SHA2_TM | HA2 |
| 1 | 0.78 (0.09) | 0.61 (0.53) | 1.58 (0.12) |
| 5 | 0.67 (0.16) | 0.89 (0.09) | 0.94 (0.25) |
| 30 | 0.92 (0.11) | 0.83 (0.16) | 0.94 (0.41) |
| 60 | 0.83 (0.00) | 0.78 (0.09) | 1.06 (0.25) |
| 120 | 0.89 (0.19) | 0.61 (0.25) | 0.94 (0.25) |

| HDX time/min | Deuterium Incorporation (%) (92-99) | | |
|---|---|---|---|
| | FHA2 | SHA2_TM | HA2 |
| 1 | 1.19 (0.41) | 3.93 (0.30) | 4.64 (0.10) |
| 5 | 1.52 (0.43) | 3.76 (0.35) | 0.90 (0.08) |
| 30 | 1.64 (0.70) | 3.62 (0.16) | 1.90 (0.86) |
| 60 | 1.64 (0.90) | 4.21 (0.50) | 2.09 (0.82) |
| 120 | 2.67 (0.70) | 1.67 (0.54) | 1.38 (0.36) |

| HDX time/min | Deuterium Incorporation (%) (99-110) | | |
|---|---|---|---|
| | FHA2 | SHA2_TM | HA2 |
| 1 | 7.48 (0.54) | 10.15 (1.99) | 4.15 (0.10) |
| 5 | 13.33 (1.42) | 18.85 (0.84) | 10.91 (0.86) |
| 30 | 18.23 (0.32) | 21.00 (1.10) | 21.15 (0.60) |
| 60 | 20.50 (0.32) | 22.09 (0.72) | 24.12 (0.19) |
| 120 | 20.97 (0.72) | 23.18 (0.51) | 25.73 (0.15) |

| HDX time/min | Deuterium Incorporation (%) (110-115) | | |
|---|---|---|---|
| | FHA2 | SHA2_TM | HA2 |
| 1 | 25.90 (1.55) | 17.13 (1.22) | 26.33 (0.61) |
| 5 | 25.40 (1.41) | 21.13 (2.51) | 28.00 (1.59) |
| 30 | 26.10 (0.14) | 22.90 (0.99) | 33.80 (0.00) |
| 60 | 29.60 (2.83) | 26.60 (1.25) | 36.50 (0.14) |
| 120 | 33.20 (0.00) | 28.20 (0.60) | 39.73 (0.61) |

| HDX time/min | Deuterium Incorporation (%) (120-138) | | |
|---|---|---|---|
| | FHA2 | SHA2_TM | HA2 |
| 1 | 38.39 (1.72) | 39.72 (0.00) | 42.50 (3.22) |
| 5 | 38.93 (1.57) | 39.83 (2.84) | 42.44 (1.86) |
| 30 | 39.56 (0.39) | 40.72 (0.02) | 42.11 (2.19) |
| 60 | 43.72 (1.26) | 42.17 (1.41) | 43.97 (0.71) |
| 120 | 45.86 (0.27) | 44.56 (3.61) | 43.03 (0.04) |

| HDX time/min | Deuterium Incorporation (%) (133-138) | | |
|---|---|---|---|
| | FHA2 | SHA2_TM | HA2 |
| 1 | 34.33 (0.94) | 33.87 (0.11) | 39.33 (0.11) |
| 5 | 34.83 (1.17) | 39.00 (1.13) | 41.73 (0.98) |
| 30 | 35.83 (0.00) | 42.93 (0.75) | 42.07 (0.46) |
| 60 | 35.94 (1.00) | 44.80 (0.69) | 43.53 (1.72) |
| 120 | 37.67 (2.02) | 45.27 (0.23) | 44.33 (1.55) |

| HDX time/min | Deuterium Incorporation (%) (139-141) | | |
|---|---|---|---|
| | FHA2 | SHA2_TM | HA2 |
| 1 | 34.50 (2.17) | 37.25 (1.76) | 31.00 (1.80) |
| 5 | 36.75 (1.06) | 46.25 (1.76) | 43.33 (3.78) |
| 30 | 46.50 (0.00) | 50.25 (1.06) | 46.83 (1.60) |
| 60 | 46.75 (0.35) | 50.75 (0.35) | 48.75 (1.06) |
| 120 | 47.75 (0.35) | 50.67 (0.28) | 49.50 (1.32) |

| HDX time/min | Deuterium Incorporation (%) (142-150) | | |
|---|---|---|---|
| | FHA2 | SHA2_TM | HA2 |
| 1 | 45.13 (0.87) | 46.63 (0.00) | 41.83 (0.14) |
| 5 | 46.04 (1.22) | 46.96 (0.14) | 44.63 (0.00) |
| 30 | 47.29 (2.30) | 49.96 (2.67) | 48.46 (0.07) |
| 60 | 47.08 (3.10) | 51.08 (0.07) | 48.38 (0.00) |
| 120 | 47.88 (0.00) | 51.04 (0.07) | 51.92 (0.14) |

| HDX time/min | Deuterium Incorporation (%) (151-162) | |
|---|---|---|
| | FHA2 | HA2 |
| 1 | 32.91 (0.00) | 30.88 (0.57) |
| 5 | 35.18 (1.41) | 34.85 (0.31) |
| 30 | 37.76 (0.10) | 40.39 (1.63) |
| 60 | 39.42 (2.93) | 41.55 (0.68) |
| 120 | 40.42 (0.05) | 42.06 (0.37) |

| HDX time/min | Deuterium Incorporation (%) (151-167) | | |
|---|---|---|---|
| | FHA2 | SHA2_TM | HA2 |
| 1 | 34.62 (0.64) | 38.21 (1.60) | 33.09 (0.75) |
| 5 | 35.87 (1.40) | 40.88 (1.92) | 34.50 (1.03) |
| 30 | 36.60 (2.15) | 41.25 (1.20) | 38.75 (1.25) |
| 60 | 38.89 (2.18) | 41.90 (0.25) | 40.33 (1.58) |
| 120 | 41.06 (1.67) | 43.79 (1.75) | 40.83 (1.43) |

| HDX time/min | Deuterium Incorporation (%) (163-167) | | |
|---|---|---|---|
| | FHA2 | SHA2_TM | HA2 |
| 1 | 36.12 (0.17) | 30.33 (0.14) | 43.75 (1.06) |
| 5 | 40.37 (3.00) | 46.12 (1.94) | 44.25 (0.25) |
| 30 | 45.50 (1.76) | 45.67 (1.84) | 45.75 (0.35) |
| 60 | 47.08 (0.14) | 46.62 (1.59) | 46.42 (1.01) |
| 120 | 47.58 (0.76) | 52.25 (1.41) | 47.00 (0.75) |

| HDX time/min | Deuterium Incorporation (%) (163-171) | | |
|---|---|---|---|
| | FHA2 | SHA2_TM | HA2 |
| 1 | 35.94 (1.67) | 33.83 (2.52) | 31.88 (1.23) |
| 5 | 37.13 (1.59) | 35.81 (2.20) | 31.19 (0.44) |
| 30 | 33.25 (3.89) | 36.71 (1.94) | 36.06 (0.08) |
| 60 | 35.50 (2.62) | 35.38 (0.79) | 35.08 (0.76) |
| 120 | 34.50 (1.06) | 35.19 (1.32) | 37.17 (0.68) |

| HDX time/min | Deuterium Incorporation (%) (168-171) | | |
|---|---|---|---|
| | FHA2 | SHA2_TM | HA2 |
| 1 | 49.22 (0.50) | 34.33 (0.88) | 39.67 (0.50) |
| 5 | 49.44 (0.38) | 55.50 (0.70) | 48.50 (0.38) |
| 30 | 50.67 (2.29) | 58.83 (1.64) | 51.44 (3.29) |
| 60 | 55.00 (2.64) | 59.22 (1.38) | 51.56 (2.65) |
| 120 | 60.56 (0.76) | 63.44 (1.34) | 53.67 (0.76) |

| HDX time/min | Deuterium Incorporation (%) (172-178) | | |
|---|---|---|---|
| | FHA2 | SHA2_TM | HA2 |
| 1 | 40.72 (0.85) | 37.33 (2.82) | 38.08 (0.82) |
| 5 | 47.25 (1.29) | 50.06 (1.10) | 43.61 (2.89) |
| 30 | 50.75 (1.06) | 50.25 (1.53) | 55.06 (1.10) |
| 60 | 53.17 (1.17) | 53.75 (3.41) | 56.06 (1.00) |
| 120 | 58.25 (0.35) | 55.39 (0.96) | 56.42 (0.35) |

| HDX time/min | Deuterium Incorporation (%) (179-187) | |
|---|---|---|
| | SHA2_TM | HA2 |
| 1 | 32.63 (0.35) | 25.63 (0.65) |
| 5 | 37.06 (1.67) | 38.75 (1.76) |
| 30 | 40.75 (1.11) | 38.38 (1.51) |
| 60 | 41.54 (1.16) | 45.08 (1.01) |
| 120 | 43.50 (0.33) | 47.50 (0.65) |

| HDX time/min | Deuterium Incorporation (%) (188-191) | |
|---|---|---|
| | SHA2_TM | HA2 |
| 1 | 6.78 (0.38) | 2.56 (0.19) |
| 5 | 6.00 (0.01) | 3.89 (0.19) |
| 30 | 10.33 (0.00) | 15.00 (0.00) |
| 60 | 15.89 (2.50) | 24.00 (0.57) |
| 120 | 17.33 (0.00) | 31.11 (0.19) |

| HDX time/min | Deuterium Incorporation (%) (192-197) | |
|---|---|---|
| | SHA2_TM | HA2 |
| 1 | 1.07 (0.64) | 2.00 (0.20) |
| 5 | 0.93 (0.30) | 1.50 (0.14) |
| 30 | 0.50 (0.14) | 2.40 (0.53) |
| 60 | 0.87 (0.11) | 2.47 (0.50) |
| 120 | 9.60 (1.41) | 2.60 (0.34) |

| HDX time/min | Deuterium Incorporation (%) (198-202/199-203) | |
|---|---|---|
| | SHA2_TM | HA2 |
| 1 | 0.88 (0.88) | 2.00 (0.17) |
| 5 | 2.17 (0.29) | 0.63 (0.17) |
| 30 | 1.17 (0.87) | 1.00 (1.52) |
| 60 | 0.88 (0.53) | 2.17 (1.44) |
| 120 | 0.83 (0.14) | 0.42 (0.14) |

| HDX time/min | Deuterium Incorporation (%) (200-202) | |
|---|---|---|
| | SHA2_TM | HA2 |
| 1 | 0.33 (0.28) | 0.00 (0.00) |
| 5 | 0.17 (0.28) | 0.17 (0.28) |
| 30 | 0.17 (0.28) | 0.17 (0.28) |
| 60 | 0.67 (0.76) | 0.17 (0.28) |
| 120 | 0.67 (0.76) | 0.17 (0.28) |

| HDX time/min | Deuterium Incorporation (%) HA2 (200-205) |
|---|---|
| 1 | 0.53 (0.23) |
| 5 | 0.40 (0.00) |
| 30 | 1.00 (0.59) |
| 60 | 1.53 (0.11) |
| 120 | 1.00 (0.20) |

| HDX time/min | Deuterium Incorporation (%)<br>HA2 (206-217) |
|---|---|
| 1 | 50.46 (2.76) |
| 5 | 54.12 (2.09) |
| 30 | 59.33 (3.22) |
| 60 | 61.50 (1.80) |
| 120 | 61.64 (1.10) |

**Tables S2**. Percent deuterium incorporation vs. HDX time for peptides from digested WT-, G1E-, and I173E- HA2. Each value is the average of triplicate measurements, and the standard deviation is given in parentheses.

| HDX time/min | Deuterium Incorporation (%) (1-8) | |
|---|---|---|
| | WT-HA2 | I173E-HA2 |
| 1 | 47.00 (1.21) | 37.14 (2.45) |
| 5 | 63.05 (0.73) | 44.79 (0.91) |
| 30 | 66.38 (1.72) | 60.00 (2.62) |
| 60 | 68.90 (1.21) | 63.29 (0.40) |
| 120 | 69.76 (0.46) | 64.21 (0.10) |

| HDX time/min | Deuterium Incorporation (%) (3-9) | |
|---|---|---|
| | G1E-HA2 | I173E-HA2 |
| 1 | 42.17 (0.94) | 42.42 (2.47) |
| 5 | 54.94 (1.86) | 49.11 (3.26) |
| 30 | 58.94 (2.77) | 59.58 (3.41) |
| 60 | 59.08 (0.82) | 62.25 (3.89) |
| 120 | 60.33 (3.49) | 63.28 (3.00) |

| HDX time/min | Deuterium Incorporation (%) (10-21) | |
|---|---|---|
| | WT-HA2 | G1E-HA2 |
| 1 | 43.58 (0.18) | 38.14 (2.51) |
| 5 | 46.09 (0.00) | 43.67 (0.50) |
| 30 | 57.05 (1.09) | 45.39 (0.71) |
| 60 | 57.07 (1.09) | 46.03 (1.08) |
| 120 | 65.59 (0.06) | 50.18 (1.98) |

| HDX time/min | Deuterium Incorporation (%) (12-22) | |
|---|---|---|
| | G1E-HA2 | I173E-HA2 |
| 1 | 43.83 (2.92) | 52.25 (3.16) |
| 5 | 45.10 (3.53) | 63.13 (4.84) |
| 30 | 49.67 (3.35) | 65.73 (0.67) |
| 60 | 51.30 (3.13) | 66.73 (0.90) |
| 120 | 59.05 (1.20) | 68.07 (0.66) |

| HDX time/min | Deuterium Incorporation (%) (22-38) | | |
|---|---|---|---|
| | WT-HA2 | G1E-HA2 | I173E-HA2 |
| 1 | 12.83 (2.02) | 14.67 (0.60) | 30.06 (1.24) |
| 5 | 15.81 (0.50) | 15.96 (1.60) | 33.34 (0.04) |
| 30 | 17.60 (1.87) | 17.15 (1.02) | 35.75 (0.89) |
| 60 | 19.69 (1.77) | 18.04 (0.65) | 37.77 (0.97) |
| 120 | 21.21 (0.22) | 20.65 (1.92) | 39.23 (1.07) |

| HDX time/min | Deuterium Incorporation (%) (39-52) | | |
|---|---|---|---|
| | WT-HA2 | G1E-HA2 | I173E-HA2 |
| 1 | 0.90 (0.22) | | 35.27 (3.86) |
| 5 | 1.56 (0.54) | | 39.36 (1.76) |
| 30 | 4.10 (0.55) | EX1 kinetics | 51.58 (0.60) |
| 60 | 4.85 (0.16) | | 53.85 (0.62) |
| 120 | 5.95 (2.05) | | 54.95 (0.42) |

| HDX time/min | Deuterium Incorporation (%) (53-69) | | |
|---|---|---|---|
| | WT-HA2 | G1E-HA2 | I173E-HA2 |
| 1 | 4.68 (0.77) | 3.21 (0.77) | 9.02 (0.12) |
| 5 | 4.63 (0.18) | 2.82 (1.30) | 16.77 (0.03) |
| 30 | 5.99 (0.61) | 4.10 (0.22) | 18.04 (0.82) |
| 60 | 6.00 (0.35) | 5.16 (1.10) | 21.53 (1.76) |
| 120 | 6.21 (0.44) | 5.33 (1.75) | 26.83 (0.64) |

| HDX time/min | Deuterium Incorporation (%) (70-87) | | |
|---|---|---|---|
| | WT-HA2 | G1E-HA2 | I173E-HA2 |
| 1 | 1.68 (0.21) | 1.03 (0.04) | 1.23 (0.35) |
| 5 | 1.68 (0.04) | 1.32 (0.12) | 1.64 (0.21) |
| 30 | 2.00 (0.17) | 1.91 (0.04) | 1.71 (0.21) |
| 60 | 2.21 (0.04) | 3.03 (1.29) | 2.03 (0.27) |
| 120 | 2.50 (0.04) | 7.35 (1.58) | 2.13 (0.20) |

| HDX time/min | Deuterium Incorporation (%) (86-91) | | |
|---|---|---|---|
| | WT-HA2 | G1E-HA2 | I173E-HA2 |
| 1 | 2.07 (1.33) | 0.20 (0.34) | 0.73 (0.46) |
| 5 | 1.93 (0.41) | 0.47 (0.42) | 0.93 (0.46) |
| 30 | 1.50 (0.14) | 3.73 (0.11) | 0.60 (0.00) |
| 60 | 3.53 (1.89) | 4.73 (1.28) | 0.93 (0.30) |
| 120 | 6.07 (1.33) | 6.67 (2.33) | 1.33 (0.81) |

| HDX time/min | Deuterium Incorporation (%) (92-98) | | |
|---|---|---|---|
| | WT-HA2 | G1E-HA2 | I173E-HA2 |
| 1 | 0.78 (0.09) | 4.17 (0.47) | 4.72 (0.19) |
| 5 | 0.67 (0.16) | 3.25 (0.11) | 4.72 (0.09) |
| 30 | 0.92 (0.11) | 4.28 (0.10) | 4.33 (0.44) |
| 60 | 0.83 (0.00) | 4.56 (0.84) | 4.44 (0.10) |
| 120 | 0.89 (0.19) | 4.33 (0.33) | 5.00 (0.29) |

| HDX time/min | Deuterium Incorporation (%) (92-99) | | |
|---|---|---|---|
| | WT-HA2 | G1E-HA2 | I173E-HA2 |
| 1 | 4.64 (0.10) | 1.48 (0.29) | 3.71 (1.61) |
| 5 | 0.90 (0.08) | 1.29 (0.51) | 2.81 (1.30) |
| 30 | 1.90 (0.86) | 1.86 (1.24) | 2.20 (1.03) |
| 60 | 2.09 (0.82) | 2.09 (1.53) | 2.43 (0.87) |
| 120 | 1.38 (0.36) | 2.86 (2.10) | 2.57 (1.51) |

| HDX time/min | Deuterium Incorporation (%) (99-110) | | |
|---|---|---|---|
| | WT-HA2 | G1E-HA2 | I173E-HA2 |
| 1 | 4.15 (0.10) | 10.00 (1.41) | 10.86 (0.32) |
| 5 | 10.91 (0.86) | 17.76 (0.58) | 12.27 (1.80) |
| 30 | 21.15 (0.60) | 18.61 (0.32) | 24.51 (2.73) |
| 60 | 24.12 (0.19) | 21.45 (1.96) | 29.06 (2.80) |
| 120 | 25.73 (0.15) | 28.79 (0.93) | 30.30 (1.59) |

| HDX time/min | Deuterium Incorporation (%) (110-115) | | |
|---|---|---|---|
| | WT-HA2 | G1E-HA2 | I173E-HA2 |
| 1 | 26.33 (0.61) | 27.07 (1.70) | 26.13 (4.52) |
| 5 | 28.00 (1.59) | 28.47 (2.14) | 33.60 (0.69) |
| 30 | 33.80 (0.00) | 32.10 (0.99) | 42.80 (1.70) |
| 60 | 36.50 (0.14) | 31.93 (1.51) | 44.07 (0.31) |
| 120 | 39.73 (0.61) | 37.60 (1.98) | 44.27 (0.42) |

| HDX time/min | Deuterium Incorporation (%) (120-138) | | |
|---|---|---|---|
| | WT-HA2 | G1E-HA2 | I173E-HA2 |
| 1 | 42.50 (3.22) | 37.88 (0.41) | 40.31 (2.87) |
| 5 | 42.44 (1.86) | 38.84 (0.48) | 45.67 (1.81) |
| 30 | 42.11 (2.19) | 39.73 (1.52) | 47.11 (0.63) |
| 60 | 43.97 (0.71) | 39.88 (1.15) | 49.41 (0.12) |
| 120 | 43.03 (0.04) | 41.01 (0.87) | 49.96 (1.67) |

| HDX time/min | Deuterium Incorporation (%) (133-138) | | |
|---|---|---|---|
| | WT-HA2 | G1E-HA2 | I173E-HA2 |
| 1 | 39.33 (0.11) | 43.30 (0.14) | 33.75 (0.82) |
| 5 | 41.73 (0.98) | 42.67 (1.20) | 36.42 (1.06) |
| 30 | 42.07 (0.46) | 42.20 (1.00) | 37.56 (1.00) |
| 60 | 43.53 (1.72) | 42.87 (0.83) | 37.50 (1.00) |
| 120 | 44.33 (1.55) | 44.07 (0.81) | 38.22 (0.42) |

| HDX time/min | Deuterium Incorporation (%) (139-141) | | |
|---|---|---|---|
| | WT-HA2 | G1E-HA2 | I173E-HA2 |
| 1 | 31.00 (1.80) | 31.17 (0.29) | 28.75 (1.77) |
| 5 | 43.33 (3.78) | 38.50 (0.00) | 40.00 (3.53) |
| 30 | 46.83 (1.60) | 39.17 (1.04) | 41.17 (1.61) |
| 60 | 48.75 (1.06) | 41.50 (2.00) | 44.00 (0.87) |
| 120 | 49.50 (1.32) | 44.17 (0.29) | 47.17 (2.93) |

| HDX time/min | Deuterium Incorporation (%) (142-150) | | |
|---|---|---|---|
| | WT-HA2 | G1E-HA2 | I173E-HA2 |
| 1 | 41.83 (0.14) | 49.00 (0.90) | 43.25 (2.65) |
| 5 | 44.63 (0.00) | 49.88 (1.02) | 46.13 (0.35) |
| 30 | 48.46 (0.07) | 50.71 (0.47) | 48.17 (0.85) |
| 60 | 48.38 (0.00) | 51.46 (0.14) | 49.75 (1.19) |
| 120 | 51.92 (0.14) | 51.83 (0.19) | 51.54 (0.29) |

| HDX time/min | Deuterium Incorporation (%) (152-167) | | |
|---|---|---|---|
| | WT-HA2 | G1E-HA2 | I173E-HA2 |
| 1 | 33.09 (0.75) | 37.41 (0.49) | 37.66 (3.67) |
| 5 | 34.50 (1.03) | 39.10 (0.24) | 44.78 (1.54) |
| 30 | 38.75 (1.25) | 40.25 (0.47) | 45.44 (0.65) |
| 60 | 40.33 (1.58) | 40.81 (0.90) | 46.90 (0.67) |
| 120 | 40.83 (1.43) | 41.29 (0.30) | 46.52 (1.15) |

| HDX time/min | Deuterium Incorporation (%) (163-167) | | |
|---|---|---|---|
| | WT-HA2 | G1E-HA2 | I173E-HA2 |
| 1 | 43.75 (1.06) | 45.50 (0.50) | 44.33 (2.63) |
| 5 | 44.25 (0.25) | 45.63 (0.53) | 47.67 (2.12) |
| 30 | 45.75 (0.35) | 46.17 (1.25) | 49.58 (0.52) |
| 60 | 46.42 (1.01) | 47.25 (0.71) | 50.50 (0.87) |
| 120 | 47.00 (0.75) | 48.67 (1.28) | 51.42 (0.52) |

| HDX time/min | Deuterium Incorporation (%) (163-171) | | |
|---|---|---|---|
| | WT-HA2 | G1E-HA2 | I173E-HA2 |
| 1 | 31.88 (1.23) | 34.83 (2.38) | 35.75 (0.53) |
| 5 | 31.19 (0.44) | 35.33 (2.00) | 37.88 (1.56) |
| 30 | 36.06 (0.08) | 36.17 (1.70) | 40.75 (1.94) |
| 60 | 35.08 (0.76) | 36.54 (2.24) | 42.04 (1.25) |
| 120 | 37.17 (0.68) | 37.08 (1.66) | 44.13 (2.14) |

| HDX time/min | Deuterium Incorporation (%) (168-171) | | |
|---|---|---|---|
| | WT-HA2 | G1E-HA2 | I173E-HA2 |
| 1 | 39.67 (1.33) | 48.44 (2.21) | 48.33 (1.88) |
| 5 | 48.50 (0.71) | 53.11 (3.59) | 54.50 (1.18) |
| 30 | 51.44 (0.19) | 55.33 (3.78) | 57.33 (3.21) |
| 60 | 51.56 (0.19) | 55.78 (5.01) | 60.11 (1.02) |
| 120 | 53.67 (0.00) | 59.00 (0.00) | 60.78 (0.77) |

| HDX time/min | Deuterium Incorporation (%) (172-178) | | |
|---|---|---|---|
| | WT-HA2 | G1E-HA2 | I173E-HA2 |
| 1 | 38.08 (0.82) | 37.08 (0.35) | 54.67 (0.94) |
| 5 | 43.61 (2.89) | 50.22 (1.51) | 58.50 (3.46) |
| 30 | 55.06 (1.10) | 51.67 (2.02) | 61.22 (1.92) |
| 60 | 56.06 (1.00) | 55.08 (0.59) | 62.61 (0.19) |
| 120 | 56.42 (0.35) | 57.67 (0.29) | 63.25 (0.11) |

| HDX time/min | Deuterium Incorporation (%) (179-187) | | |
|---|---|---|---|
| | WT-HA2 | G1E-HA2 | I173E-HA2 |
| 1 | 25.63 (0.65) | 39.25 (2.47) | 36.96 (1.73) |
| 5 | 38.75 (1.76) | 40.00 (1.77) | 47.04 (1.58) |
| 30 | 38.38 (1.51) | 41.42 (0.56) | 52.13 (1.96) |
| 60 | 45.08 (1.01) | 44.96 (2.94) | 54.88 (2.54) |
| 120 | 47.50 (0.65) | 48.31 (2.21) | 57.88 (2.51) |

| HDX time/min | Deuterium Incorporation (%) (188-191) | | |
|---|---|---|---|
| | WT-HA2 | G1E-HA2 | I173E-HA2 |
| 1 | 2.56 (0.19) | 12.67 (3.77) | 16.33 (1.41) |
| 5 | 3.89 (0.19) | 25.67 (1.15) | 18.00 (4.58) |
| 30 | 15.00 (0.00) | 30.67 (1.33) | 37.00 (2.02) |
| 60 | 24.00 (0.58) | 32.00 (1.45) | 40.89 (0.84) |
| 120 | 31.11 (0.19) | 34.00 (3.30) | 48.33 (1.76) |

| HDX time/min | Deuterium Incorporation (%) (192-197) | | |
|---|---|---|---|
| | WT-HA2 | G1E-HA2 | I173E-HA2 |
| 1 | 2.00 (0.20) | 0.87 (0.30) | 1.00 (0.34) |
| 5 | 1.50 (0.14) | 0.87 (0.64) | 0.93 (0.23) |
| 30 | 2.40 (0.53) | 1.40 (0.20) | 1.27 (0.11) |
| 60 | 2.47 (0.50) | 1.13 (0.30) | 1.53 (0.11) |
| 120 | 2.60 (0.35) | 1.07 (0.23) | 1.80 (0.20) |

| HDX time/min] | Deuterium Incorporation (%) (198-202/199-203) | | |
|---|---|---|---|
| | WT-HA2 | G1E-HA2 | I173E-HA2 |
| 1 | 2.00 (0.17) | 0.25 (0.00) | 3.58 (2.98) |
| 5 | 0.63 (0.17) | 2.00 (3.03) | 0.33 (0.14) |
| 30 | 1.00 (1.52) | 4.17 (3.39) | 0.25 (0.00) |
| 60 | 2.17 (1.44) | 0.25 (0.00) | 0.25 (0.00) |
| 120 | 0.42 (0.14) | 4.00 (3.30) | 3.75 (3.03) |

| HDX time/min | Deuterium Incorporation (%) (200-202) | | |
|---|---|---|---|
| | WT-HA2 | G1E-HA2 | I173E-HA2 |
| 1 | 0.00 (0.00) | 0.00 (0.00) | 0.00 (0.00) |
| 5 | 0.17 (0.28) | 0.00 (0.00) | 0.50 (0.00) |
| 30 | 0.17 (0.28) | 0.00 (0.00) | 0.00 (0.00) |
| 60 | 0.17 (0.28) | 0.00 (0.00) | 0.00 (0.00) |
| 120 | 0.17 (0.28) | 0.00 (0.00) | 0.17 (0.29) |

| HDX time/min | Deuterium Incorporation (%) (206-217) | | |
|---|---|---|---|
| | WT-HA2 | G1E-HA2 | I173E-HA2 |
| 1 | 50.46 (2.76) | 52.36 (1.52) | 45.80 (3.74) |
| 5 | 54.12 (2.09) | 53.42 (0.54) | 51.99 (0.31) |
| 30 | 59.33 (3.22) | 57.92 (0.54) | 57.04 (1.86) |
| 60 | 61.50 (1.80) | 58.40 (0.37) | 61.03 (1.47) |
| 120 | 61.64 (1.10) | 60.72 (1.44) | 62.31 (2.27) |

**Figure S2.** Structural models of WT-, I173E-, and G1E- HA2 in a single membrane. The HA2 structures are the same as in Fig. 8. The approximate locations of specific residues are noted.

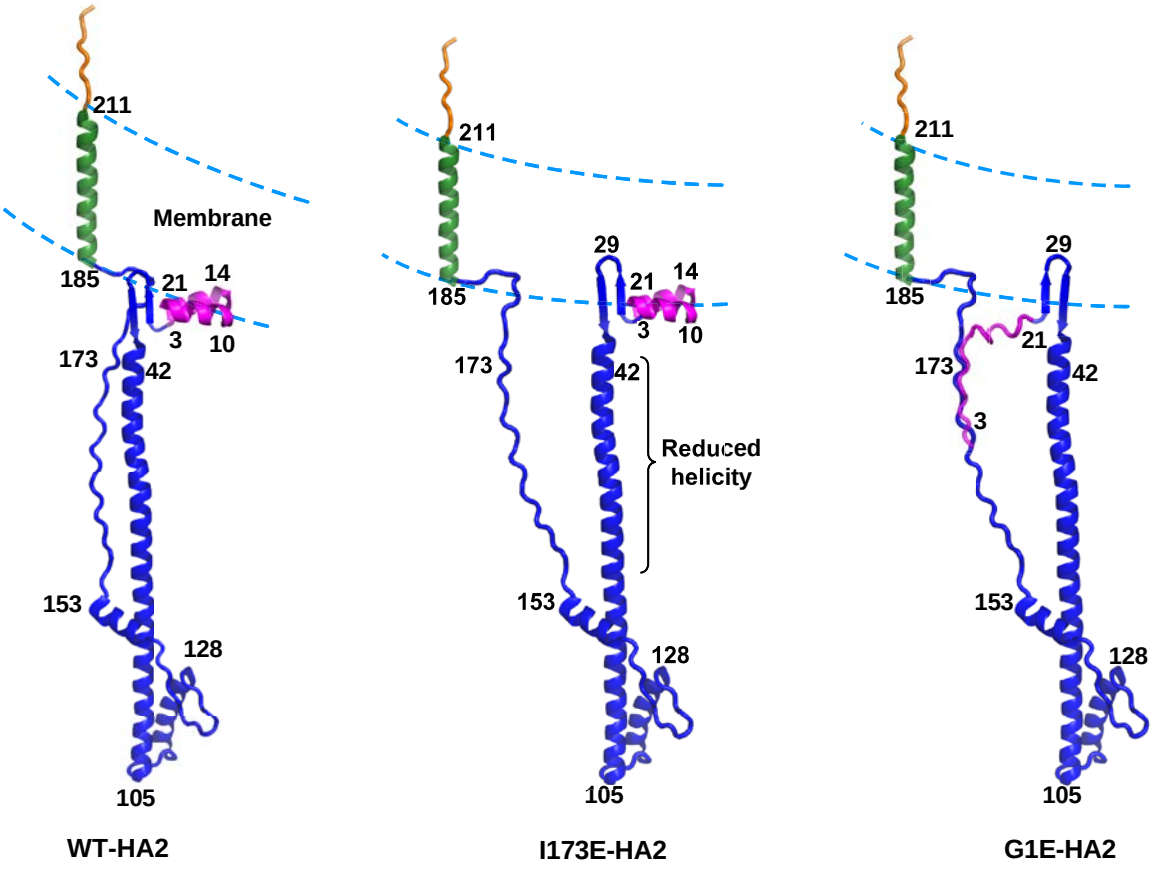

**Table S3**. Percent deuterium incorporation vs. HDX time for the 39-52 peptide of WT-, I173E-, and G1E- HA2. WT and I173E exhibit approximately unimodal distributions in the m/z = 496-501 range, and G1E exhibits a bimodal distribution for $t_{HDX}$ = 120 min, with the modes approximately separable into m/z = 496-498 and 498-501 ranges. Each value is the average of triplicate measurements, and the RMSD is given in parentheses. $\langle D_{\%} \rangle$ is the average of the five $D_{\%}$, and the associated uncertainty in parentheses is calculated using the $D_{\%}$ RMSD's.

| HDX time/min | Protein (m/z range) | | | |
|---|---|---|---|---|
| | WT-HA2 (496-501) | I173E-HA2 (496-501) | G1E-HA2 (496-498) | G1E-HA2 (498-501) |
| 1 | 0.90 (0.22) | 35.27 (3.86) | 6.89 (0.11) | 66.21 (0.66) |
| 5 | 1.56 (0.54) | 39.36 (1.76) | 7.15 (0.28) | 65.18 (0.75) |
| 30 | 4.10 (0.55) | 51.58 (0.60) | 7.23 (0.35) | 65.44 (0.83) |
| 60 | 4.85 (0.16) | 53.85 (0.62) | 15.37 (0.21) | 65.52 (1.24) |
| 120 | 5.95 (2.05) | 54.95 (0.42) | 16.23 (0.96) | 62.83 (1.32) |
| | | | | |
| $\langle D_{\%} \rangle$ | 3.26 (0.23) | 47.00 (0.87) | 10.58 (0.22) | 65.04 (0.45) |

**Figure S3.** Comparison between $D_{\%}$ of the present study and an earlier study for $t_{HDX}$ = 1 min and $t_{HDX}$ = 30 min (*Structure* (2015) **23**, 665-676). Data are displayed for peptides respectively from FHA2 ≡ $HA2_{1\text{-}185}$ and from the $HA2_{1\text{-}175}$/HA1 complex after incubation at pH 4.9 for three hours.